# Palmitoylated Importin α Regulates Mitotic Spindle Orientation Through Interaction with NuMA

**Authors**

Patrick James Sutton[1,*] and Christopher W. Brownlee[1,2]

**Author Affiliations and Footnotes**

[1]Department of Pharmacological Sciences, Stony Brook University; Stony Brook, 11794, United States of America.

[2]Lead Contact

*Correspondence: Patrick.Sutton@stonybrook.edu (P.J.S), Christopher.Brownlee@stonybrook.edu (C.W.B)

## Abstract

Regulation of cell division orientation is a fundamental process critical to differentiation and tissue homeostasis. Microtubules emanating from the mitotic spindle pole bind a conserved complex of proteins at the cell cortex which orients the spindle and ultimately the cell division plane. Control of spindle orientation is of particular importance in developing tissues, such as the developing brain. Misorientation of the mitotic spindle and thus subsequent division plane misalignment can contribute to improper segregation of cell fate determinants in developing neuroblasts, leading to a rare neurological disorder known as microcephaly. We demonstrate that the nuclear transport protein importin α, when palmitoylated, plays a critical role in mitotic spindle orientation through localizing factors, such as NuMA, to the cell cortex. We also observe craniofacial developmental defects in *Xenopus laevis* when importin α palmitoylation is abrogated, including smaller head and brains, a hallmark of spindle misorientation and microcephaly. These findings characterize not only a role for importin α in spindle orientation, but also a broader role for importin α palmitoylation which has significance for many cellular processes.

## Introduction

Mitotic spindle orientation is a fundamental cellular process which regulates cell division orientation, a crucial aspect of mitosis that when dysregulated can lead to uncontrolled asymmetric division and overproliferation, or developmental defects due to premature stem cell differentiation, depending on the cell type (Bergstralh and St Johnston, 2014; Bergstralh et al., 2017; Charnley et al., 2013; Finegan and Bergstralh, 2019). Neuronal development in particular is heavily reliant on properly oriented cell divisions to ensure the correct timing of neuron

differentiation, a process that when disturbed can result in severe defects, such as microcephaly (Razuvaeva et al., 2023; Higgins and Goldstein, 2010; Konno et al., 2008).

Mitotic spindle orientation is largely controlled by the anchoring of astral microtubules (aMTs) to the cell cortex in metaphase, and the pulling force generated by the dynein/dynactin motor complex on aMTs during anaphase (Kiyomitsu and Cheeseman, 2012; Kotak and Gönczy, 2013; Toyoshima and Nishida, 2007; Pietro et al., 2016; Bergstralh et al., 2017; Singh et al., 2021; Yang et al., 2014). aMTs are anchored at the cortex by a conserved complex of proteins consisting of Gαi, which through myristylation is thought to associate with the plasma membrane (PM), Leucine-Glycine-Asparagine repeat containing protein (LGN), which binds to Gαi, and Nuclear Mitotic Apparatus (NuMA), which binds to LGN and dynein/dynactin, facilitating the strong pulling force on the aMTs necessary for maintenance of spindle orientation in metaphase (Higgins and Goldstein, 2010; Pietro et al., 2016; Camuglia et al., 2022; Kiyomitsu and Cheeseman, 2012; Fankhaenel et al., 2023; He et al., 2023; Kiyomitsu and Boerner, 2021; Zheng et al., 2013; Okumura et al., 2018; Pirovano et al., 2019; Du and Macara, 2004; Neville et al., 2022; Yu et al., 2000; Bowman et al., 2006; Carvalho et al., 2015). While all of these factors play a role in aMT anchoring during metaphase, only NuMA and dynein/dynactin are required during anaphase to ensure the proper separation of chromatin to the poles (Bergstralh and St Johnston, 2014). Additionally, it has been shown that LGN and Gαi are only required for NuMA localization to the cell cortex during metaphase, not anaphase (Okumura et al., 2018; Kiyomitsu and Boerner, 2021). However, it remains unclear how these factors localize to the PM during metaphase and how this membrane localization is maintained there when it is believed that only a singly myristoylated Gαi is responsible for membrane association of the entire aMT anchoring complex. The necessity for a significant pulling force towards the PM during metaphase to orient

57 the mitotic spindle and during anaphase to facilitate separation of chromatin to the poles suggests
58 that an additional factor, which can associate with the PM via multiple interaction points, may be
59 playing a role in aMT anchoring.

60 Importin α is known for functioning as a nuclear transport adapter in interphase and as a
61 spindle assembly factor during mitosis through its ability to bind Nuclear Localization Signal
62 (NLS) sequence containing proteins (Takeda et al., 2011; Oka and Yoneda, 2018; Goldfarb et al.,
63 2004). However in recent years, a number of proteomic screens for palmitoylated proteins
64 utilizing a variety of biochemical methods and mass spectrometry verification have identified
65 human importin α-1 (KPNA2) as a target for palmitoylation (Won and Martin, 2018; Thinon et
66 al., 2018; Serwa et al., 2015; Mariscal et al., 2020; Schelar and Liu, 2008; Zhou et al., 2019;
67 Sobocinska et al., 2018). Palmitoylation is a reversible and dynamic process which modifies
68 proteins post translationally with palmitate lipids allowing both diffusion and vesicle mediated
69 transport of palmitoylated proteins to the PM (Guan and Fierke, 2011). Additionally, recent work
70 in *Xenopus laevis* (*X. laevis*) revealed that importin α can be reversibly sequestered to the PM
71 via palmitoylation of 4 key residues, 3 of which are conserved in humans (Brownlee and Heald,
72 2019). This same study found that when palmitoylated, importin α acts as an evolutionarily
73 conserved cell-surface area-to-volume sensor that coordinately scales nuclear and spindle size to
74 cell size. Following this work, mass spectrometry methods have confirmed palmitoylation of at
75 least one cysteine in human KPNA2 in addition to the 3 residues conserved from *X. laevis*
76 importin α-1 (Zhou et al., 2019) and palmitoylation prediction screens have identified additional
77 cysteine residues in human KPNA2 likely to be palmitoylated with high confidence. These
78 findings raise the intriguing possibility that importin α may have roles other than as a nuclear
79 import adapter upon palmitoylation (Brownlee and Heald, 2019).

80 Due to the requirement of an exceedingly strong pulling force to drive orientation of the
81 spindle and chromatin separation to the poles, we hypothesize that palmitoylated importin α
82 could provide a sufficiently strong interaction with the PM to anchor aMTs in mitosis. Importin
83 α when modified with palmitate lipids at multiple residues would provide a significantly
84 increased membrane association compared to singly myristoylated Gαi and could increase the
85 membrane association of the aMT anchoring complex as a whole if bound to the factors
86 involved. Notably, NuMA as well as Discs Large (Dlg), another protein recently implicated in
87 spindle orientation (Bergstralh et al., 2016; Carvalho et al., 2015; Saadaoui et al., 2014; Schiller
88 and Bergstralh, 2021), contain strongly predicted NLS sequences suggesting importin α may be
89 responsible for their cellular localization through importin α-NLS binding. Previous literature
90 has also investigated the effects of deleting the NLS of NuMA and determined that NuMA's NLS
91 is required for its cortical localization (Okumura et al., 2018). Additionally, findings which
92 demonstrate that NuMA does not require LGN or Gαi to localize to the polar cortex during late
93 anaphase raise the intriguing possibility that palmitoylated importin α may play a role in
94 NuMA's mitotic localization. We hypothesize that palmitoylated importin α could bind NuMA's
95 NLS in metaphase, transport it to the PM and therefore be necessary for NuMA's localization in
96 metaphase and early anaphase, and sufficient for NuMA's localization during late anaphase
97 (Okumura et al., 2018; Kiyomitsu and Boerner, 2021).
98 A key factor driving protein localization and spindle formation in mitosis is a gradient of
99 RanGTP generated by the chromosome-tethered RanGEF, RCC1 (Kalab and Heald, 2008). In
100 interphase, the same localized concentration of RanGTP in the nucleus facilitates release of cargo
101 from importins for proper nuclear transport (Kalab and Heald, 2008; Ozugergin and Piekny,
102 2021). All of these processes are driven by the binding of RanGTP to importin β, which causes

103 the dissociation of importins and any bound cargo (Kalab and Heald, 2008; Oka and Yoneda,
104 2018). In mitosis, chromosomes are arranged during metaphase in such a manner that the
105 tethered RCC1 generates a high concentration of RanGTP at the midline of the cell, but a low
106 concentration of RanGTP towards the poles (Ems-McClung et al., 2020). The lack of RanGTP at
107 the polar cortex and the abundance of RanGTP at the lateral cortex during metaphase due to the
108 equatorial localization of the mitotic Ran gradient indicates that importin α can remain bound to
109 NLS containing cargo at the polar cortex exclusively. Importantly, this is where aMTs are
110 anchored and NuMA has been found to localize (Kiyomitsu and Cheeseman, 2012; Oka and
111 Yoneda, 2018; Chang et al., 2017; Kalab and Heald, 2008; Ems-McClung et al., 2020). This
112 suggests that the Ran gradient can regulate the localization of NLS containing proteins at the PM
113 and therefore restrict localization of NuMA to the polar cortex, through interaction with
114 palmitoylated importin α. Additionally, it has been shown that manipulation of the Ran gradient
115 disrupts spindle orientation and the localization of spindle orientation factors (Kiyomitsu and
116 Cheeseman, 2013).

117 In the present work we demonstrate that importin α when palmitoylated is a key regulator
118 of mitotic spindle orientation through localization of NuMA to the PM during metaphase and as
119 such palmitoylation of importin α is required for proper control of cell division orientation. We
120 show that palmitoylated importin α can localize throughout the PM in mitotic cells and that
121 palmitoylation of importin α is required for both proper spindle orientation and proper NuMA
122 localization in metaphase. While importin α localizes to the entire PM when palmitoylated (at
123 both the lateral and polar cortex), the accumulation of RanGTP near the metaphase plate would
124 preclude importin α binding to NuMA, leading to accumulation of NuMA specifically to the
125 polar cortex, where aMTs are anchored. We also explore the effects of importin α palmitoylation

disruption on neuronal development in *X. laevis* and observe microcephaly which can be rescued upon forcing importin α to the PM independent of palmitoylation, further supporting that PM localization of palmitoylated importin α is a key regulator of mitotic spindle orientation.

## Results

### Importin α Localizes to The Mitotic Polar Cortex at Metaphase in a Palmitoylation-Dependent, but Not Cargo-Dependent Manner

Importin α has long been recognized for its role in spindle assembly during mitosis by facilitating the transport of spindle assembly factors to the midline of the cell, where mitotic spindles form (Kalab and Heald, 2008; Kaláb et al., 2006; Weaver and Walczak, 2015; Goldfarb et al., 2004). However, recent work has demonstrated in *X. laevis* that importin α can be post translationally modified with palmitate lipids to drive PM localization (Brownlee and Heald, 2019). These palmitoylation sites are conserved in human importin α and additional palmitoylation sites have been confirmed by palmitoylation prediction screens (Supplemental Figure 1A) and multiple mass spectrometry studies of global palmitoylated proteins (Mariscal et al., 2020; Zhou et al., 2019; Won and Martin, 2018; Thinon et al., 2018; Serwa et al., 2015; Sobocinska et al., 2018). Additionally, NLS prediction screens have shown an enrichment of NLS containing proteins which localize to the PM and play a role in a variety of cellular processes, including spindle orientation (Supplemental Figure 1B&C).This suggests that palmitoylated importin α may be involved in mitotic cellular processes outside of spindle assembly at the PM by binding NLS containing proteins and localizing them there.

We sought to investigate other possible roles of palmitoylated importin α in mitosis by either increasing or decreasing levels of palmitoylated importin α, as well as inhibiting importin

150 α's ability to bind or release cargo. To manipulate palmitoylation of importin α, we targeted the
151 specific proteins responsible for palmitoylating and depalmitoylating importin α. Palmitoylation
152 is catalyzed by palmitoyl acyl transferases (PATs), which attach palmitoyl groups to serine or
153 cysteine residues, while depalmitoylation is carried out by acyl protein thioesterases (APTs)
154 which remove palmityl groups (Guan and Fierke, 2011). To modulate palmitoylation levels
155 specifically, we used small molecule inhibitors to target porcupine (PORCN), the serine PAT
156 responsible for palmitoylation of serine residues on importin α, and APT1, the APT responsible
157 for depalmitoylation of importin α (Brownlee and Heald, 2019). HCT116 colorectal cancer cells
158 were selected for this study due to their established role as a model system for both spindle
159 orientation and NuMA localization (Okumura et al., 2018; Tsuchiya et al., 2021).

160 We investigated the role of importin α in palmitoylation-mediated PM targeting using
161 HCT116 cells synchronized in metaphase and treated with either DMSO (control) or Wnt-C59, a
162 competitive inhibitor of PORCN (Proffitt et al., 2013). Wnt-C59 treatment would be expected to
163 result in a reduction in cellular palmitoylated importin α levels, leading to a decrease in the
164 population of importin α localized to the PM. Conversely, palmostatin treatment, which inhibits
165 APT1 (Dekker et al., 2010; Lin and Conibear, 2015), would be expected to result in an increase
166 in palmitoylated importin α levels, known as hyper-palmitoylation, which would increase the
167 population of importin α localized to the PM.

168 Mitotic importin α cellular localization was assessed after 1 hour in the respective drug
169 treatments, with cell boundaries determined by bright-field microscopy (Supplemental Figure 2).
170 In DMSO control cells, importin α is observed localizing to centrosomes, near the assembling
171 spindles, and at the PM (Figure 1A). Notably, Wnt-C59 treatment resulted in a 6-fold decrease of
172 importin α signal at the PM and a concurrent enrichment of importin α signal in the cytoplasm

173 (Figure 1A-D), while palmostatin treatment did not alter importin α PM localization compared to
174 DMSO control treatment (Figure 1A-D). PM localization in DMSO control cells was confirmed
175 by western blot analysis of subcellular-fractioned HCT116 cells. HCT116 cells were metaphase
176 arrested and fractionated into 4 fractions: nuclear, cytoplasmic, organelles, and PM. The PM and
177 cytoplasmic fractions were analyzed by SDS-PAGE and immunoblotted for β-tubulin, as a
178 cytoplasmic marker, plasma membrane $Ca^{2+}$ ATPase1 (PMCA1), as a PM marker, and importin
179 α. β-tubulin was detected only in the cytoplasmic fraction and PMCA1 was detected only in the
180 PM fraction demonstrating proper isolation of cellular fractions. However, importin α was
181 detected in both the cytoplasmic and PM fractions confirming our immunofluorescence findings
182 that importin α localizes to the PM in metaphase-arrested cells (Figure 1E). These results
183 collectively suggest that palmitoylation of importin α during metaphase is required for its proper
184 localization to the cortex.

185 The localization of importin α during metaphase was also analyzed in the presence of
186 drugs that disrupt its ability to bind and release cargo. Metaphase-arrested HCT116 cells were
187 treated with either ivermectin, a small molecule inhibitor that prevents the binding of importin α
188 to NLS containing cargoes (Wagstaff et al., 2012) or importazole, a small molecule inhibitor of
189 importin based nuclear transport that prevents RanGTP mediated release of cargo from importins
190 (Soderholm et al., 2011) (Figure 1A-D). We observed that in both importazole and ivermectin
191 treated cells, importin α remained unperturbed at the PM (Figure 1A-D). Notably, in all drug
192 treatments mitotic spindles were still formed properly despite disruption of importin α
193 palmitoylation or NLS cargo binding. Taken together, these results suggest importin α partitions
194 to the mitotic cortex via palmitoylation and does not require binding of NLS-containing cargoes
195 to localize to the PM.

196 **Importin α Palmitoylation and Cargo Binding Is Required for Proper Mitotic Spindle**
197 **Orientation**

198 We next sought to determine the effect of both disrupting importin α's ability to properly
199 bind NLS-containing cargo and importin α mislocalization on the orientation of the metaphase
200 mitotic spindle. HCT116 cells were metaphase-arrested and treated with DMSO, Wnt-C59,
201 palmostatin, importazole, ivermectin, or 2-bromopalmitate, a pan palmitoylation inhibitor (Lin
202 and Conibear, 2015). The angle of the metaphase spindle was then calculated using the relative
203 horizontal and vertical distances between the two spindle poles (Figure 1F). Mitotic spindles
204 were found to be misoriented in all treatments other than palmostatin relative to the DMSO-
205 treated control (Figure 1G & H). Interestingly, disruption of importin α palmitoylation (Wnt-C59
206 treatment), which was previously shown to alter mitotic importin α localization, and disruption
207 of importin α's ability to properly bind and release cargo (ivermectin and importazole treatments
208 respectively) both resulted in spindle misorientation. These data suggest that importin α
209 palmitoylation is required for proper spindle orientation, and spindle orientation is dependent
210 upon importin α binding of NLS-containing cargo.

211 To determine if the spindle misorientation phenotypes observed when HCT116 cells were
212 treated with palmitoylation disrupting drugs were specifically due to mislocalization of importin
213 α from the cell cortex, we constructed a plasmid containing importin α modified with a C-
214 terminal CaaX domain. Addition of the CaaX domain to importin α facilitates its cortical
215 localization through farnesylation, irrespective of its palmitoylation status (Supplemental Figure
216 3). Unlike palmitoylation, farnesylation is irreversible, enabling CaaX-modified proteins to be
217 directed to the membrane and remain tethered there(Tang et al., 2009; Tamanoi et al., 2001).
218 HCT116 cells were transfected via nucleofection to express CaaX-modified importin α or an

219 unmodified importin α 24 hours prior to metaphase arrest and subsequent drug treatment with
220 DMSO or Wnt-C59. We observed that HCT116 cells overexpressing unmodified importin α
221 exhibited significantly misoriented spindle structures when treated with Wnt-C59 compared to
222 DMSO treatment (Figure 1I). However, HCT116 cells overexpressing CaaX-modified importin
223 α did not exhibit misorientation of spindle structures under the same conditions (Figure 1I),
224 therefore rescuing spindle misorientation in Wnt-C59 treatment. This suggests that the spindle
225 misorientation phenotypes observed when palmitoylation is disrupted are specifically due to
226 mislocalization of importin α to the mitotic cell cortex.

227 Several cancer cell lines have been shown to harbor various mutations which exacerbate
228 mitotic spindle orientation phenotypes (Chhabra and Booth, 2021). Therefore, we repeated the
229 previous spindle orientation experiment using an hTERT immortalized cell line, RPE-1, treated
230 with Wnt-C59 and palmostatin (Figure 1J). We again observed that Wnt-C59, but not palmostatin
231 treatment resulted in mitotic cells with significantly misoriented spindle structures relative to the
232 DMSO control (Figure 1K). This confirmed the findings in HCT116 cells and further suggests
233 that palmitoylation of importin α is required for proper mitotic spindle orientation.

234 **Importin α Interacts with NuMA but not Dlg at the Metaphase Cell Cortex**

235 Mitotic spindle orientation in vertebrates is mediated through aMT anchoring at the cell
236 cortex via a conserved protein complex consisting of LGN, Gαi, NuMA and dynein/dynactin
237 (Bergstralh et al., 2017); additionally, while the membrane protein Dlg has also been implicated
238 in spindle orientation, its exact interaction within this complex is unknown. Of these known
239 spindle orientation proteins, only NuMA and Dlg contain predicted and conserved NLS
240 sequences and are thus potential binding partners of importin α.

241 We therefore sought to probe if importin α can directly bind to either of these proteins at
242 the mitotic cortex using a rolling amplification based proximity ligation assay (PLA) (Alam,
243 2018). Importin α interaction with NuMA or Dlg was quantified by measuring the number of
244 PLA foci in 3 regions of interest at the polar cortex, lateral cortex, and in the cytoplasm to
245 determine where in the cell these proteins were interacting (Figure 2A). PLA was performed on
246 metaphase-arrested HCT116 cells in DMSO control, Wnt-C59 and palmostatin treated conditions
247 using specific antibodies to importin α and either NuMA or Dlg (Figure 2B and C, respectively).
248 The assay revealed that importin α and NuMA interact at the polar cortex of DMSO treated
249 metaphase cells, but not Wnt-C59 treated cells. Additionally, NuMA and importin α interactions
250 were found at both the polar and lateral cortices in palmostatin treated cells (Figure 2D).
251 Palmostatin treated cells also exhibited a marked enrichment of importin α-NuMA interactions at
252 the centrosomes and along spindle structures (Figure 2D) suggesting that importin α could
253 associate more strongly with NuMA when hyper-palmitoylated. It is noteworthy that importin α
254 and NuMA were only found to interact at the polar cortex in control conditions as we have
255 previously demonstrated that palmitoylated importin α localizes throughout the mitotic PM at
256 both the polar and lateral cortex (Figure 1A). This is to be expected, as although importin α is
257 present throughout the cortex, the presence of the RanGTP gradient at the midline of the cell
258 prevents importin α from binding or remaining bound to the NLS of NuMA at the lateral cortex,
259 limiting their interaction to the polar cortex where aMTs are anchored.

260 When probing for importin α interaction with Dlg, we observed that while importin α
261 and Dlg were found to interact throughout the cytosol, this interaction was not enriched at any
262 specific cellular location and was not altered by Wnt-C59 or palmostatin treatment (Figure 2E).
263 These results collectively suggest that precise importin α palmitoylation levels are required to

264 maintain the importin α-NuMA interaction at the mitotic polar cortex and that importin α and
265 Dlg do not interact at the PM. A potential explanation for importin α interacting with NuMA
266 specifically and not Dlg is that these proteins contain distinct NLS sequences, such that NuMA
267 has a bipartite NLS while Dlg is predicted to have a monopartite NLS (Chang et al., 2017). It is
268 plausible that palmitoylated importin α, which would need to bind to these proteins in order to
269 localize them to the membrane, binds preferentially to some NLS containing cargo over others.

270 We then confirmed the importin α/NuMA interaction via immunoprecipitation of the
271 endogenous proteins from metaphase-arrested HCT116 cells treated with DMSO, Wnt-C59 and
272 palmostatin (Figure 2F). While importin α and NuMA were found to associate in all conditions,
273 interestingly, hyper-palmitoylated importin α due to palmostatin treatment resulted in an
274 approximately 4X increase in NuMA association, suggesting that palmitoylation status
275 influences importin α cargo-binding. The observations of increased importin α-NuMA
276 interaction at centrosomes when importin α is hyper-palmitoylated (Figure 2B) and of increased
277 importin α-NuMA binding when hyper-palmitoylated (Figure 2F) could be due to the
278 palmitoylated residues of importin α lying within the NLS binding domain (Brownlee and
279 Heald, 2019). Specifically, cysteine 223 (palmitoylated residue confirmed by mass spectrometry)
280 and cysteine 237 (palmitoylated residue conserved from *X. laevis*) of human KPNA2 lies within
281 the major NLS binding domain which may partially occlude the major NLS binding site
282 affecting palmitoylated importin α's ability to bind some cargoes.

283 To account for potential differences in NuMA or importin α protein levels after drug
284 treatments, we performed a western blot and found that none of the treatments altered protein
285 levels in metaphase-arrested HCT116 cells (Figure 2G, H & I). Taken together, these results

286 suggest that importin α interacts with NuMA at the mitotic polar cortex in a palmitoylation-
287 dependent manner.

288 **NuMA Localization During Metaphase is Dependent on Its Ability to Bind Palmitoylated**
289 **Importin α**

290 It has previously been shown that deletion of NuMA's NLS causes mislocalization of
291 NuMA away from the polar cortex (Okumura et al., 2018). Based on this and our findings that
292 importin α palmitoylation is required for proper spindle orientation, we reasoned that importin α
293 may be driving NuMA's mitotic localization to the polar cortex through binding NuMA's NLS
294 and anchoring it to the PM. We next sought to determine how disruption of importin α
295 palmitoylation and its ability to properly bind and release cargo could affect NuMA's mitotic
296 localization.

297 Metaphase-arrested HCT116 cells expressing mClover-NuMA were treated with
298 palmitoylation and importin α cargo binding altering drugs and analyzed for NuMA localization
299 in metaphase (Figure 3A). NuMA intensity was measured at three cellular locations (polar
300 cortex, lateral cortex, and cytoplasm). To account for cell-to-cell differences in fluorescent
301 intensity these measurements were normalized by calculating the ratio of polar cortex/lateral
302 cortex, polar cortex/cytoplasm, and lateral cortex/cytoplasm fluorescent intensities. In the DMSO
303 control there is an enrichment of NuMA at the polar cortex over the lateral cortex as has been
304 previously characterized (Kiyomitsu and Boerner, 2021). It is worth noting that while importin α
305 localizes to the PM at both the lateral and polar cortices (Figure 1A), NuMA only localizes to the
306 polar cortex in control conditions (Figure 3A). This is expected as the RanGTP gradient at the
307 midline of the cell would prevent NLS containing cargo, such as NuMA, from remaining bound
308 to importin α at the lateral cortex. Strikingly, NuMA polar cortex enrichment was lost in all drug

309 conditions (Figure 3B). In Wnt-C59 and ivermectin treated cells, NuMA localization shifts away
310 from the polar cortex and is instead enriched in the cytoplasm compared to the DMSO control
311 (Figure 3C). In palmostatin and importazole treated cells, NuMA localization no longer enriched
312 at the polar cortex, but rather localized throughout the cortical membrane, including the lateral
313 cortex (Figure 3D). This unexpected lateral cortex localization when importin α is hyper-
314 palmitoylated upon palmostatin treatment, or cannot release cargo upon importazole treatment,
315 suggests that importin α may be an upstream regulator of proper NuMA localization at the polar
316 cortex. These results suggest that palmitoylated importin α membrane localization and cargo
317 binding is necessary for NuMA's localization and maintenance to the mitotic polar cortex.

318 **Disruption of Importin α Palmitoylation Results in Microcephaly Phenotypes in *X. laevis***

319 Having established the role of palmitoylated importin α in mitotic spindle orientation by
320 localizing NuMA to the polar cortex and maintaining it there, we subsequently sought to validate
321 these findings in vivo. Numerous centrosomal and mitotic spindle orientation defects have been
322 linked to microcephaly, as the resulting misorientation of cell division during brain development
323 leads to a depletion of neuroprogenitor cells, and consequently, total brain tissue at the
324 completion of development (Bergstralh and St Johnston, 2014). The African clawed frog
325 *Xenopus laevis* has been used extensively as a model system to study microcephaly and
326 developmental craniofacial abnormalities (Kennedy and Dickinson, 2014; Lasser et al., 2019;
327 Shantanam and MUELLER, 2018). Consequently, we utilized this model organism to determine
328 whether mislocalization of importin α at the PM and subsequent spindle misorientation might
329 lead to microcephaly or microcephaly-associated phenotypes. Leveraging our in vitro
330 observations, we analyzed the effects of disrupting mitotic spindle orientation by abrogating
331 importin α palmitoylation in the developing *X. laevis* model system.

332 *X. laevis* eggs were fertilized, placed in drug baths containing DMSO, Wnt-C59 or
333 palmostatin at approximately NF stage 24 and allowed to develop until NF stage 42 when
334 craniofacial measures can first be made (Figure 4A) (Kennedy and Dickinson, 2014; Shantanam
335 and MUELLER, 2018). Drug treated *X. laevis* embryos were assessed for craniofacial defects by
336 three metrics: distance between eyes, snout length and overall head area. Embryos were
337 immobilized in MS-222 and imaged from a dorsal perspective allowing for direct measurement
338 of cranial morphometrics. Both Wnt-C59 and palmostatin treatments significantly altered all
339 three metrics of head shape/size (Figure 3B) indicating that precise importin α palmitoylation is
340 required for proper craniofacial development in *X. laevis*. In addition to alterations in head shape,
341 drug treated tadpoles also exhibited other body morphology defects. Notably, Wnt-C59 treated
342 tadpoles exhibited much smaller tails than other conditions and a much higher mortality rate than
343 other conditions (Supplemental Figure 4).

344 While craniofacial abnormalities are a hallmark of microcephaly, we wanted to directly
345 measure potential microcephaly phenotypes. We therefore sought to quantify the neuroprogenitor
346 population in the various drug treated *X. laevis* tadpoles. DMSO, Wnt-C59 and palmostatin
347 treated *X. laevis* embryos were analyzed at NF stage 46, when brain development expansion
348 reaches its apex (Exner and Willsey, 2021) by immunostaining for nestin, a neuroprogenitor
349 marker (Suzuki et al., 2010). Immunofluorescence images were taken of tadpole forebrains and
350 analyzed for the number of total cells, determined by DNA signal, that were positive for nestin,
351 indicating a neuroprogenitor identity (Figure 4C). Due to higher mortality rate in Wnt-C59
352 treated *X. laevis* embryos, no Wnt-C59 treated tadpoles survived to NF stage 46 to be analyzed,
353 indicative of severe developmental defects in both the brain and other tissue. Palmostatin treated
354 *X. laevis* embryos survived to NF stage 46 at the same rate as DMSO controls but exhibited a

355 significantly diminished neuroprogenitor population (Figure 4D). While total cell count remained
356 the same from DMSO to palmostatin treatments, the number of nestin positive cells decreased
357 (Figure 4D). This decrease in neuroprogenitors at NF stage 46 suggests that the morphometric
358 defects observed previously are indicative of true microcephaly, which is characterized by
359 defects in neuroprogenitor population maintenance.

360 To further characterize the observed microcephaly phenotypes NF stage 42 drug treated
361 *X. laevis* embryos were analyzed for the number of phosphohistone 3 (PH3) positive cells, a
362 marker for actively dividing cells (Elmaci et al., 2018), in the brain. Embryos treated with
363 DMSO or Wnt-C59 were wholemount immunostained for DNA and PH3 and imaged via
364 confocal microscopy to determine the number of cells positive for PH3 in the brain (Figure 5A).
365 Wnt-C59 treated embryos exhibited a 6-fold decrease in the number of actively dividing cells
366 compared to DMSO control conditions (Figure 5D). Additionally, Wnt-C59 treated embryos at
367 NF stage 42 displayed deformed brains which lacked mid and forebrain patterning. These results
368 together with our morphometric measurements indicate that dysregulation of palmitoylation
369 causes craniofacial defects and particularly microcephaly in *X. laevis* embryos.

370 **Forcing Importin α to the PM Rescues *X. laevis* Microcephaly Phenotypes Observed When**
371 **Palmitoylation is Disrupted**

372 Up to this point we have exclusively altered importin α palmitoylation using small
373 molecule inhibitors, such as Wnt-C59 and palmostatin. Wnt-C59, however, exhibits off-target
374 effects by inhibiting the PAT PORCN, which palmitoylates Wnt for secretion in addition to
375 importin α. Given the crucial role of Wnt signaling in stemness and whole body development in
376 *X. laevis* (Yu et al., 2024), it is plausible that the observed effects in Wnt-C59-treated embryos
377 are off-target effects and cannot be directly attributed to importin α palmitoylation. Critically, to

378 address these off-target effects we investigated whether the loss of mitotic cells in the brain
379 leading to microcephaly was specifically caused by inhibiting importin α palmitoylation. To this
380 end, we utilized CaaX-modified importin α to force it to the cell membrane independently of
381 palmitoylation. Previously, we demonstrated that expression of CaaX-modified importin α could
382 rescue spindle misorientation phenotypes induced by Wnt-C59 treatment in human cell culture
383 (Figure 1E). By forcing importin α to the cell membrane while importin α palmitoylation is
384 abrogated, we can determine whether the microcephaly phenotype observed in Wnt-C59-treated
385 *X. laevis* embryos is specifically attributable to the absence of membrane-bound importin α or
386 other off-target effects.

387 We found that when *X. laevis* embryos were injected with CMV promoter-driven
388 wildtype and CaaX importin α exhibited increased mortality and developmental defects likely
389 due to overexpression associated issues (Supplemental Figure 5). To combat this, an importin α-
390 CaaX construct was developed in a tetracycline inducible vector, pcDNA4TO, that would allow
391 for titratable levels of importin α expression. Additionally, we mitigated global developmental
392 defects of importin α overexpression by targeting expression exclusively to the D11 blastomere
393 which is fated to give rise to the brain (Moody, 1987a; b*). X. laevis* embryos were co-injected
394 with importin α-CaaX pcDNA4TO and a plasmid expressing the tet repressor at the D11
395 blastomere and analyzed for potential rescue of microcephaly (Figure 5B).

396 Importantly, *X. laevis* embryos microinjected with importin α-CaaX pcDNA4TO at the
397 D11 blastomere and treated with Wnt-C59 exhibited a rescue of PH3 levels in the brain at NF
398 stage 42 compared to uninjected Wnt-C59 treated embryos (Figure 5D). Additionally, the
399 microinjected tadpoles exhibited brain morphology more similar to the canonical brain
400 morphology at this stage, as seen in the DMSO control, than compared with the uninjected Wnt-

401 C59 treated embryos (Figure 5A&B). When treated with Wnt-C59, Importin α-CaaX injected
402 embryos showed brain PH3 levels about 2.5 times higher than both uninjected embryos and
403 embryos injected at D11 with an mCherry tagged CaaX domain (Figure 5C&D). Taken together,
404 these results suggest that disrupting importin α palmitoylation leads to a loss of dividing cells in
405 the developing *X. laevis* brain, which subsequently causes microcephaly. Furthermore, the
406 expression of the membrane-bound importin α CaaX construct, but not the uninjected, or
407 mCherry CaaX constructs, can rescue both brain cell proliferation and attenuate microcephaly in
408 *X. laevis* compared to drug treatment alone. This finding aligns with our in vitro work in cell
409 culture, where forcing importin α to the cell cortex was able to rescue spindle misorientation
410 (Figure 1I). These findings demonstrate that the membrane localization of importin α is
411 sufficient to rescue palmitoylation disruption-induced spindle misorientation in vitro and
412 microcephaly in vivo.
413
414 **Discussion**
415 Importin α is known to act almost exclusively as a nuclear transport protein by binding
416 NLS sequence containing proteins. In the present study we have demonstrated a previously
417 uncharacterized role for importin α at the PM. We have shown that importin α, when partitioned
418 to the PM via palmitoylation, plays a crucial role in mitotic spindle orientation. Disruption of
419 importin α palmitoylation resulted in mitotic spindle misorientation and mislocalization of the
420 aMT anchoring protein NuMA. While LGN and Gαi are necessary to ensure proper spindle
421 orientation in metaphase (Bergstralh et al., 2017; Neville et al., 2022; Zhong et al., 2022), we
422 have shown that importin α, while palmitoylated, is also required for proper NuMA localization
423 and in turn proper spindle orientation, irrespective of LGN and Gαi. Our finding that importin α

424 plays a role in spindle orientation through interaction with the aMT anchoring complex is
425 especially noteworthy in that importin α's ability to bind cargo is sensitive to the RanGTP
426 gradient which emanates from the chromatin. As NuMA is a known cargo of importin α and has
427 been shown in this work to interact with palmitoylated importin α at the polar cortex, this
428 provides a regulatory pathway by which the localization of the chromatin and the RanGTP
429 gradient can determine where aMTs are anchored. This relationship is able to explain the well-
430 defined spatial organization of the aMT anchoring complex exclusively to the polar cortex which
431 has been shown to be essential for proper spindle orientation (Bergstralh et al., 2017)(Figure 6).
432 Our results demonstrated that disruption of importin α palmitoylation leads to
433 developmental defects in *X. laevis* embryos, specifically microcephaly. Defects in neurogenesis,
434 in particular microcephaly, have long been linked to spindle misorientation(Taverna et al., 2014).
435 Neuroprogenitors rely on proper spindle orientation to correctly align polarity cues which
436 regulate cell fate determination in the developing brain (Taverna et al., 2014). During early
437 neurogenesis, neuroprogenitors rely on several symmetric divisions to generate a large enough
438 population of cells to later divide asymmetrically and differentiate into neurons. Spindle
439 misorientation can cause neuroprogenitors to prematurely differentiate, depleting the pool of
440 neuroprogenitors, resulting in an overall decrease in neuronal tissue and microcephaly (Taverna
441 et al., 2014; Razuvaeva et al., 2023). Expression of importin α modified with a CaaX motif,
442 which is forced to the PM by farnesylation, effectively rescued both the spindle misorientation
443 observed in HCT116 cells and the developmental defects observed in *X. laevis*. These findings
444 further emphasize the role of palmitoylated importin α in spindle orientation and neurogenesis.
445 The observed rescues not only demonstrate importin α's involvement in aMT anchoring, but also
446 that the spindle misorientation and microcephaly observed when palmitoylation was disrupted by

447 Wnt-C59 treatment are not due to off-target effects and can be attributed, in part, to
448 mislocalization of importin α from the PM, as those phenotypes are reversed by forcing importin
449 α to the PM.

450 We propose an updated model for mitotic spindle orientation in which aMT anchoring at
451 the cell cortex is mediated by palmitoylated importin α through its interaction with NuMA
452 (Figure 6). In this newly proposed model, the RanGTP gradient plays a significant role in
453 limiting the binding of NuMA to palmitoylated importin α to the polar cortex exclusively. This
454 provides a mechanism by which palmitoylated importin α can regulate spindle orientation by
455 binding directly to NuMA with spatial binding cues provided by the RanGTP gradient emanating
456 from the chromosomes at the metaphase plate (Figure 6). Further studies to explore NuMA
457 activation via phosphorylation, which has been previously linked with NuMA PM localization
458 and association with the aMT anchoring complex of proteins (Gallini et al., 2016), and its impact
459 on binding to palmitoylated importin α would be beneficial to expand this model and provide a
460 robust view of NuMA localization in mitosis. It is reasonable to hypothesize that phosphorylated
461 NuMA could bind with differential preference to palmitoylated importin α similar to our
462 observation that hyper-palmitoylation of importin α increased NuMA/importin α interaction, but
463 this warrants further study and remains speculative.

464 The present work not only highlights the importance of importin α as a key upstream
465 regulator in mitotic spindle orientation, but also serves as the first evidence of a novel protein
466 transport pathway by which palmitoylated importin α can transport NLS containing proteins to
467 the PM. This new transport pathway could be involved in several cellular processes due to the
468 abundance of NLS containing proteins that enrich at the PM and provides a potential new level
469 of regulation of these processes through regulation of importin α palmitoylation. Overall, our

work challenges the long-standing dogma of importin α only facilitating transport into the nucleus and suggests that there are a number of potential non-canonical roles for importin α at the membrane.

**Acknowledgements**

We thank Natalie Mosqueda, Kathryn Malone, and Melanie Garcia for their constructive feedback on this work, engaging discussions, and edits during the writing of this manuscript. We thank Maurice Kernan, Holly Colognato, Gerald Thomsen, and Daniel Levy for their insights and suggestions on experimental approach. We thank the Stony Brook University Central Microscopy Imaging Center (CMIC) and Guowei Tian for assistance in imaging with Zeiss LSM 980 Airsycan 2 NLO Two-Photon Confocal Microscope. Work was supported by National Institutes of Health grant 1R35GM147569-01 (C.W.B).

**Author Contributions**

C.W.B initially conceptualized the project. P.J.S and C.W.B designed the project. P.J.S performed all experiments and analysis of data. P.J.S prepared the figures, and P.J.S and C.W.B wrote the manuscript. C.W.B procured funding for this project.

**Declaration of Interests**

The authors declare no competing interests.

**Figures**

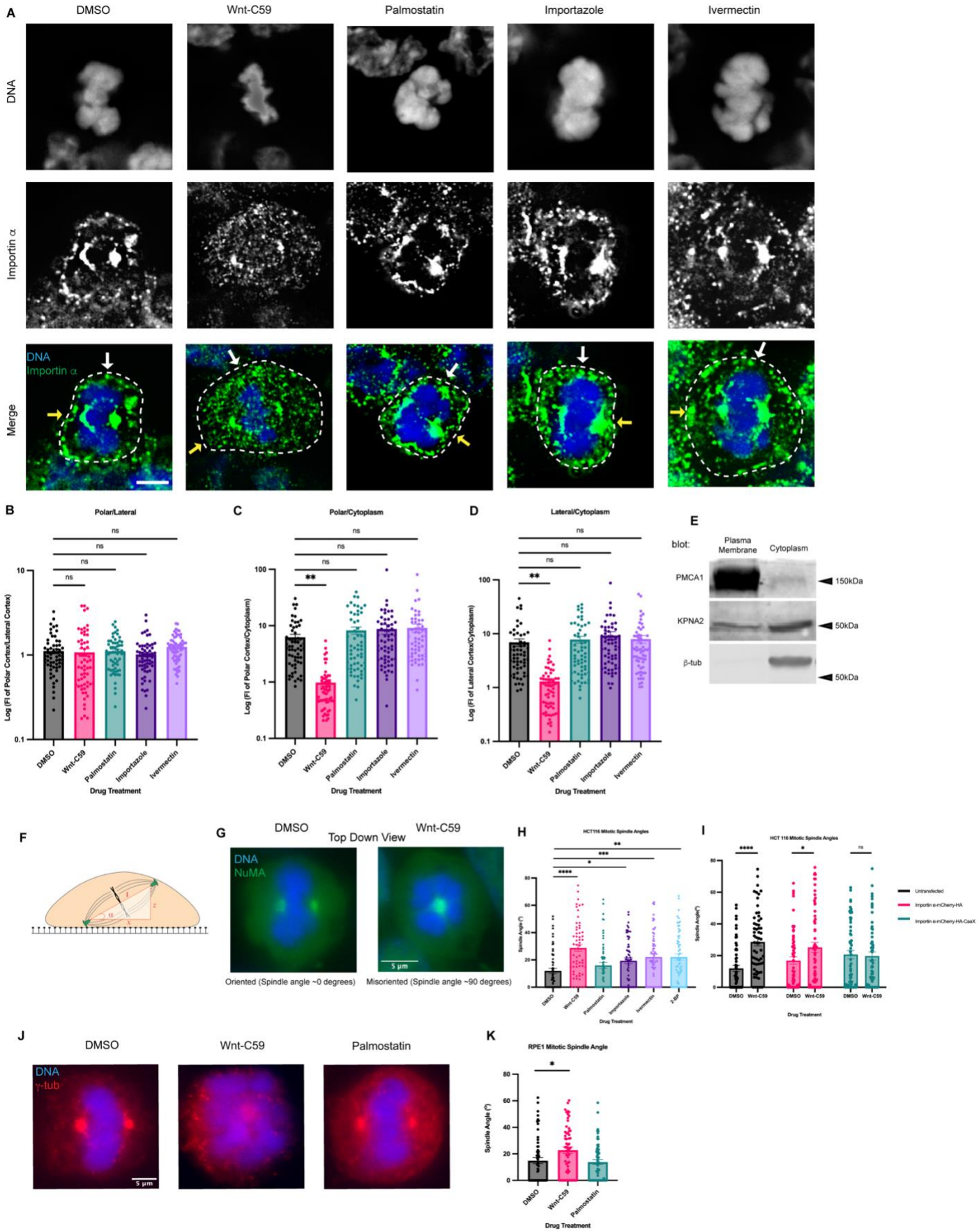
A
DMSO
Wnt-C59
Palmostatin
Importazole
Ivermectin
DNA
Importin α
Merge
DNA
Importin α
B
Polar/Lateral
Log (FI of Polar Cortex/Lateral Cortex)
Drug Treatment
C
Polar/Cytoplasm
Log (FI of Polar Cortex/Cytoplasm)
D
Lateral/Cytoplasm
Log (FI of Lateral Cortex/Cytoplasm)
E
blot:
Plasma Membrane
Cytoplasm
PMCA1
KPNA2
β-tub
150kDa
50kDa
50kDa
F
G
DMSO
Top Down View
Wnt-C59
DNA
NuMA
5 µm
Oriented (Spindle angle ~0 degrees)
Misoriented (Spindle angle ~90 degrees)
H
HCT116 Mitotic Spindle Angles
Spindle Angle (°)
Drug Treatment
I
HCT 116 Mitotic Spindle Angles
Untransfected
Importin α-mCherry-HA
Importin α-mCherry-HA-CaaX
J
DMSO
Wnt-C59
Palmostatin
DNA
γ-tub
5 µm
K
RPE1 Mitotic Spindle Angle
Spindle Angle (°)
Drug Treatment

492

493 **Figure 1. Palmitoylation Mediated Cortical Localization of Importin α and Importin α**
494 **Cargo Binding are Required for Proper Mitotic Spindle Orientation.**
495 A) Immunofluorescence images of importin α localization in metaphase-arrested (refer to
496 Materials & Methods) HCT116 cells incubated for 1 hour with DMSO, drugs that inhibit
497 importin palmitoylation (10μM Wnt-C59) drugs that enhance importin palmitoylation (50μM
498 palmostatin), and drugs that inhibit importin cargo binding (25μM ivermectin) or cargo release
499 (40μM importazole). Yellow arrows indicate cortical poles and white arrows indicate lateral
500 cortex. Scale bar=5μm. Cell boundaries determined by brightfield.
501 B-D) Quantification of importin α localization in drug treated cells. Measurements of importin
502 α signal intensity were made at three cellular locations: polar cortex, lateral cortex and
503 cytoplasm. Polar cortex measurements were made for each cell at the pole with the higher
504 measure of intensity, a similar method was used for lateral cortex measurements and cytoplasm
505 measurements were made at the midline of the cell. These measurements were normalized to
506 each other on a cell-by-cell basis by determining the ratio of cortical vs lateral importin α,
507 cortical vs cytosolic importin α, and lateral vs cytosolic importin α. Mean +/- SEM n=60 from 2
508 replicates **=$p<0.01$.
509 E) Western blot of HCT116 cell fractions following subcellular fractionation to separate PM,
510 cytoplasmic, organelle, and nuclear fractions. PM and cytoplasmic fractions shown. Western
511 blots were immunostained for PMCA1 (PM marker), β-tubulin (cytoplasmic marker), and
512 importin α (KPNA2).
513 F) Cartoon representation of a metaphase cell with misoriented spindles mounted on a coverslip
514 indicating the angle, α, which was measured as the arctangent of the horizontal distance, z, over

515 the vertical distance, x, between the two centrosomes to determine the angle of spindle
516 structures.
517 G) Immunofluorescence images of metaphase-arrested HCT116 cells in presence of DMSO or
518 10μM Wnt-C59 stained for NuMA. DMSO treated cell represents a properly oriented cell with a
519 spindle angle of 0 degrees relative to the parallel of the coverslip the cells were mounted on.
520 Wnt-C59 treated cell represents a severely misoriented cell with a spindle angle of 90 degrees
521 relative to the parallel of the coverslip the cells were mounted on. Scale bar=5μm
522 H) Quantification of mitotic spindle angles for metaphase-arrested HCT116 cells incubated in
523 DMSO, 10μM Wnt-C59, 50μM palmostatin, 40μM importazole, 25μM ivermectin, or 100μM 2-
524 bromopalmitate for 1 hour prior to analysis. All drug treatments except palmostatin significantly
525 increased the mean spindle angle of metaphase cells relative to a DMSO control. Mean +/- SEM,
526 n=60 mitotic cells from 2 replicates *=p<0.05 **=p<0.01 ***=p<0.001 ****=p<0.0001. Refer
527 to Materials & Methods for method of determining spindle angle.
528 I) Quantification of mitotic spindle angles for metaphase-arrested HCT116 cells incubated with
529 DMSO or 10μM Wnt-C59 expressing importin α-mCherry-HA or importin α-mCherry-HA-
530 CaaX. Cells expressing importin α-mCherry-HA-CaaX showed no spindle misorientation when
531 treated with Wnt-C59. Mean +/- SEM, n=60 mitotic cells from 2 replicates *=p<0.05
532 ****=p<0.0001.
533 J) Immunofluorescence images of metaphase-arrested RPE-1 cells incubated with DMSO, 10μM
534 Wnt-C59, or 50μM palmostatin for 1 hour prior to analysis stained for γ-tubulin. DMSO treated
535 cells are representative of cells with properly oriented spindles. Wnt-C59 treated cells were
536 significantly misoriented and palmostatin treated cells were properly oriented when compared to
537 DMSO control. Scale bar=5μm

538 K) Quantification of mitotic spindle angles for metaphase-arrested RPE-1 cells incubated with

539 DMSO, 10μM Wnt-C59 or 50μM palmostatin for 1 hour prior to analysis. Wnt-C59 treatment

540 significantly increased the mean spindle angle of metaphase cells relative to a DMSO control

541 while palmostatin treatment did not significantly increase the mean spindle angle relative to a

542 DMSO control. Mean +/- SEM, n=60 mitotic cells from 2 replicates *=p<0.05.

543

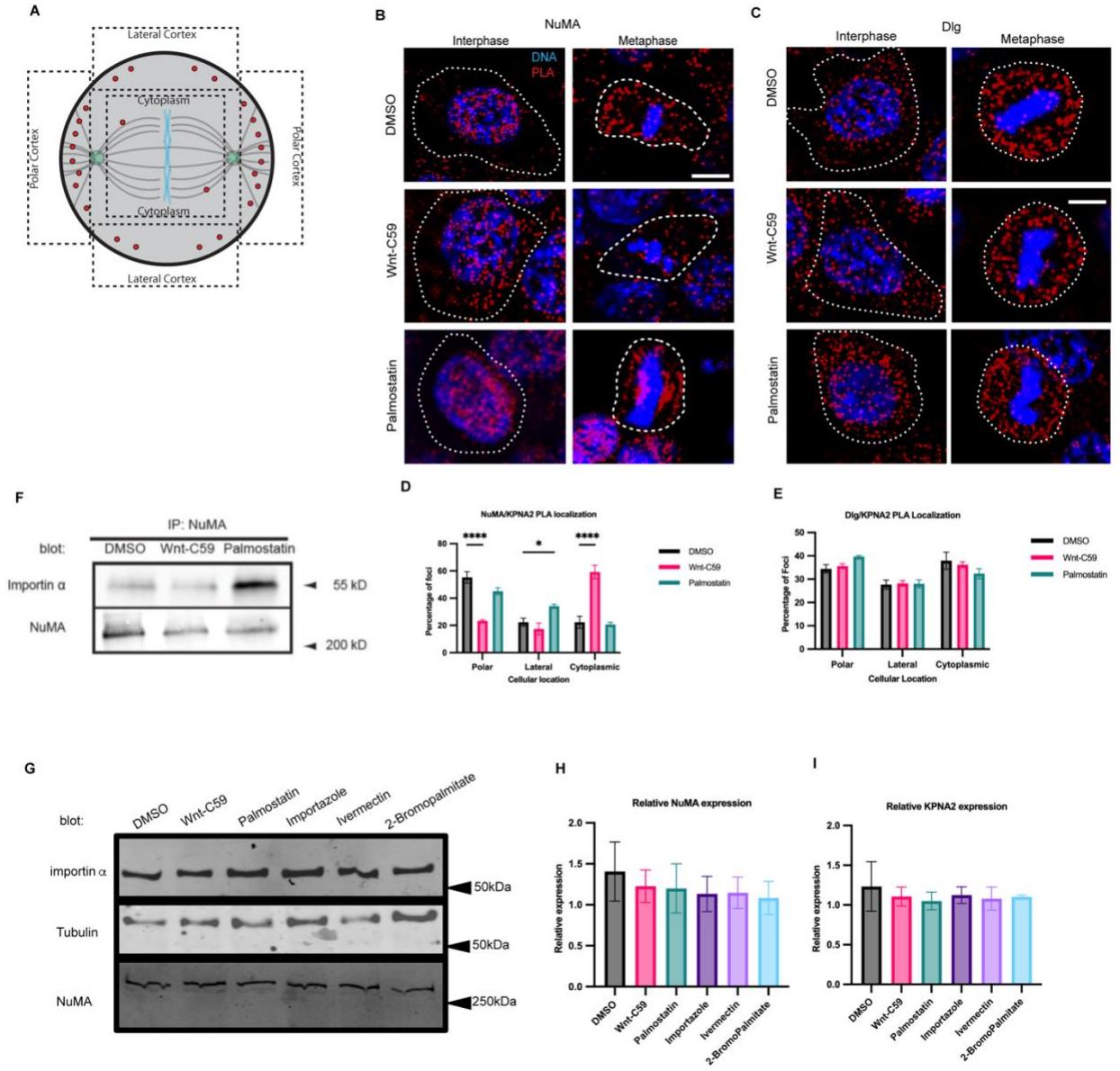


544

545 **Figure 2. Importin α Interacts with NuMA, but not Dlg at the Metaphase Cell Cortex in a**
546 **Palmitoylation Dependent Manner.**
547 A) Cartoon schematic of PLA quantification. ROIs of quantification represented by dashed lines.
548 B) Immunofluorescence images of DuoLink proximity ligation assay probing interaction of
549 NuMA with importin α (KPNA2) in interphase and metaphase-arrested HCT116 cells in the
550 presence of DMSO, 10μM Wnt-C59 or 50μM palmostatin for 1 hour prior to analysis. White
551 dashed lines indicate cell borders as determined by brightfield images. Scale bar=5μm.
552 C) Immunofluorescence images of DuoLink proximity ligation assay probing interaction of Dlg
553 with importin α (KPNA2) in interphase and metaphase-arrested HCT116 cells in the presence of
554 DMSO, 10μM Wnt-C59 or 50μM palmostatin. White dashed lines indicate cell borders. Scale
555 bar=5μm.
556 D) Quantification of the percentage of importin α (KPNA2)-NuMA PLA foci at the polar cortex,
557 lateral cortex and cytoplasm in DMSO, Wnt-C59 and palmostatin treated cells. Foci was
558 enriched at the polar cortex in DMSO treated cells, the cytoplasm in Wnt-C59 treated cells, and
559 the lateral cortex in palmostatin treated cells. Mean +/- SEM, n>136 foci *=p<0.05
560 ****=p<0.0001
561 E) Quantification of the percentage of importin α (KPNA2)-Dlg PLA foci at the polar cortex,
562 lateral cortex and cytoplasm in DMSO, Wnt-C59 and palmostatin treated cells. Localization of
563 PLA foci did not change across three drug treatments. Mean +/- SEM, n>297 foci
564 F) Western blot of NuMA Immunoprecipitation from HCT116 cells treated with DMSO, 10μM
565 Wnt-C59 or 50μM palmostatin for 1 hour prior to analysis. Immunoprecipitation of NuMA
566 followed by importin α and NuMA western blot.

567 G) Western blot of importin α, NuMA and β-tubulin in metaphase-arrested HCT116 cells in the

568 presence of DMSO, 10μM Wnt-C59, 50μM Palmostatin, 40μM importazole, 25μM ivermectin,

569 or 100μM 2-bromopalmitate.

570 H and I) Quantification of NuMA and importin α (KPNA2) expression levels respectively,

571 relative to β-tubulin protein levels for each condition.

572

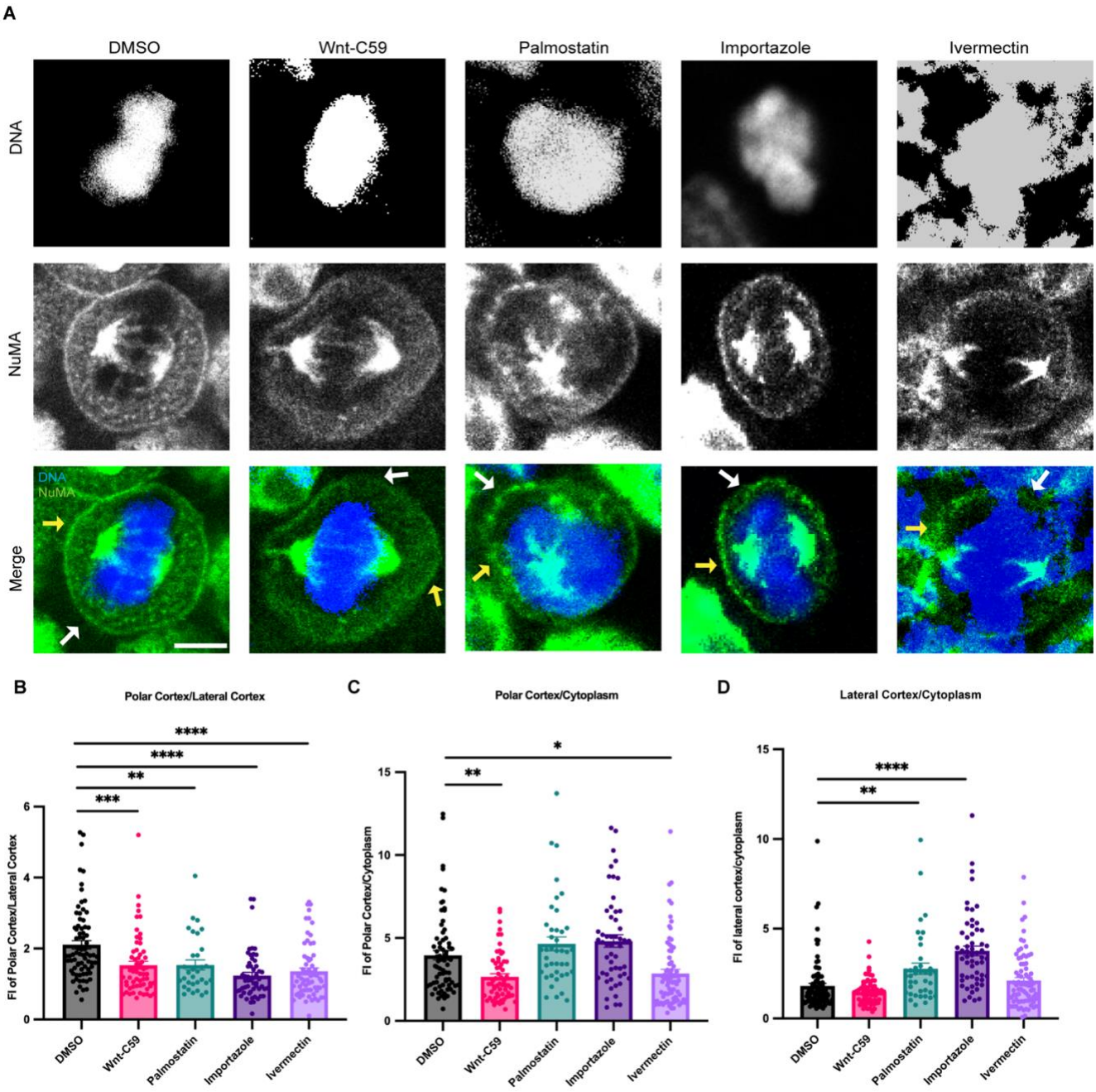


**Figure 3. Palmitoylated Importin α Regulates Cortical Localization of NuMA in Metaphase.**

A) Confocal images of NuMA localization in metaphase-arrested HCT116 cells in the presence of DMSO, 10μM Wnt-C59, 50μM palmostatin, 40μM importazole or 25μM ivermectin. Yellow arrows indicate cortical poles and white arrows indicate lateral cortex. Scale bar=5μm.

B-D) Quantification of NuMA localization in drug treated cells. Measurements of NuMA signal intensity were made at three cellular locations: polar cortex, lateral cortex and cytoplasm. Polar cortex measurements were made for each cell at the pole with the higher measure of intensity, a similar method was used for lateral cortex measurements and cytoplasm measurements were made at the midline of the cell. These measurements were normalized to each other on a cell-by-cell basis by determining the ratio of polar vs lateral NuMA, polar vs cytosolic NuMA, and lateral vs cytosolic NuMA. Mean +/- SEM n>40 *=p<0.05 **=p<0.01 ***=p<0.001 ****=p<0.0001.

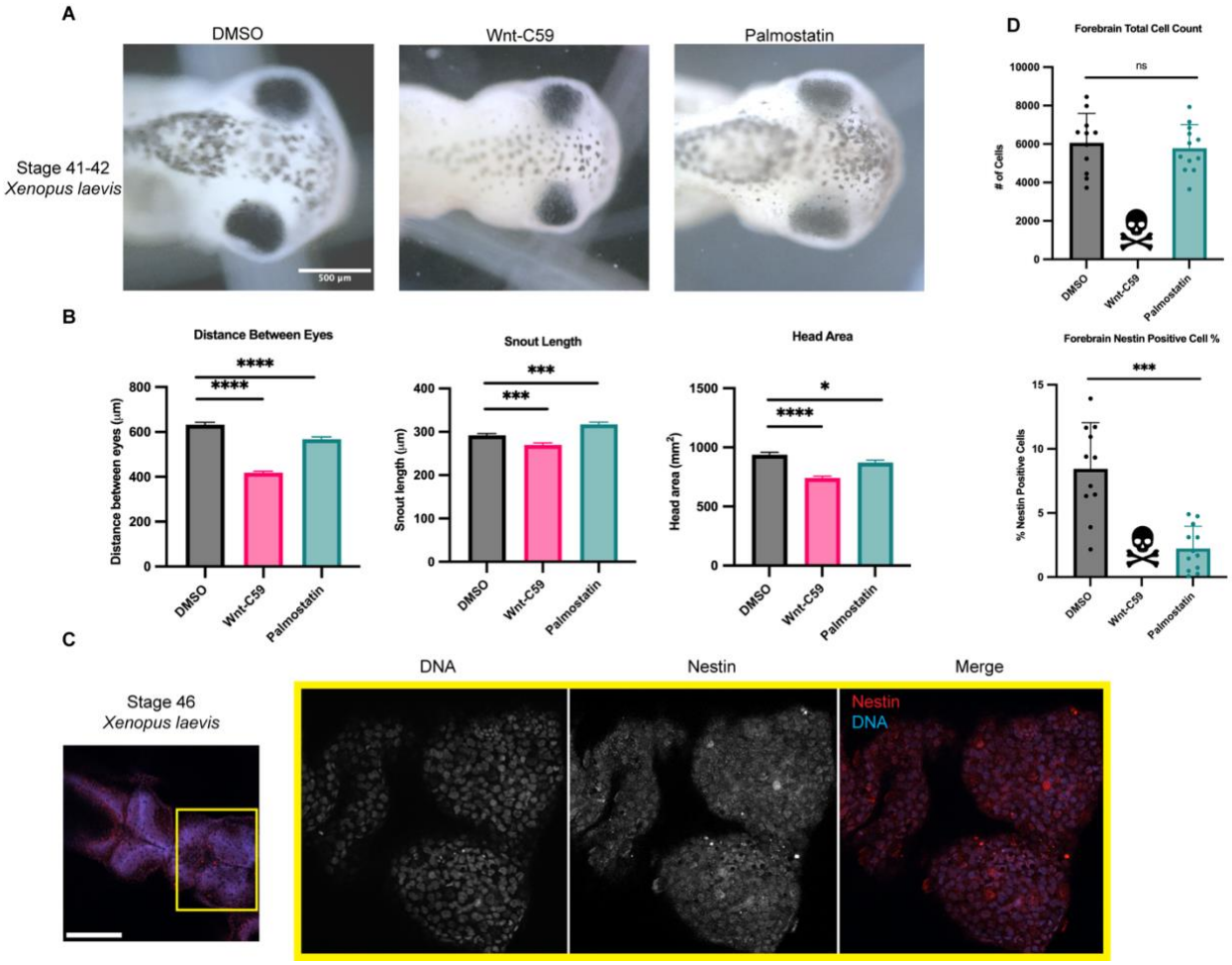

589 **Figure 4. Regulation of Palmitoylation is Required for Proper Brain Development in**

590 ***Xenopus laevis*.**

591 A) Bright field images of stage 42 *X. laevis* grown in the presence of DMSO, 100μM Wnt-C59

592 or 1mM palmostatin. Scale bar=500μm

593 B) Measurements of drug treated stage 42 *X. laevis* head shape by 3 metrics: distance between

594 eyes, snout length, and overall head area. Mean +/- SEM n>55 *=p<0.05 ***=p<0.001

595 ****=p<0.0001. All 3 metrics of head shape were significantly altered from DMSO control in

596 both Wnt-C59 and palmostatin treatments.

597 C) Immunofluorescence images of DMSO treated stage 46 *X. laevis* immunostained for the

598 neuroprogenitor marker nestin and stained with Hoechst to visualize DNA. Scale bar=250μm.

599 D) Quantification of total cell count in forebrains and percentage of forebrain cells positive for

600 nestin signal in stage 46 *X. laevis* grown in the presence of DMSO, 100μM Wnt-C59 or 1mM

601 palmostatin. Quantifications were performed on maximum projection images from z-stack

602 images of *X. laevis* brains with a parent-child analysis to determine the number of total cells as

603 determined by Hoechst signal that also were positive for nestin signal. Mean +/- SEM n=12

604 ***=p<0.001. All Wnt-C59 treated *X. laevis* died before reaching stage 46 while all palmostatin

605 treated *X. laevis* display a significantly reduced neuroprogenitor population by nestin positive

606 cell count.

607

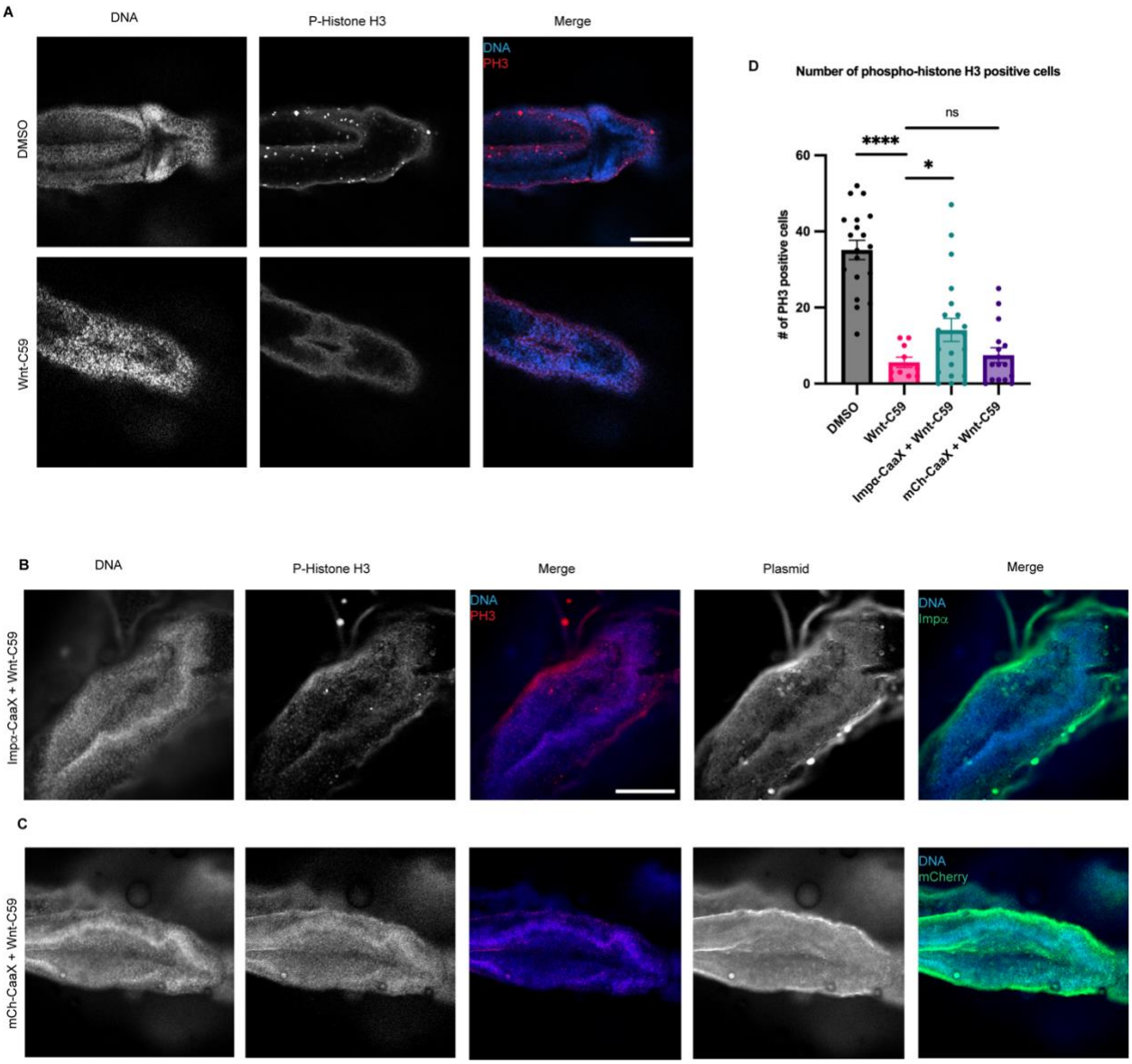


**Figure 5. Overexpression of CaaX Modified Importin α in the Developing *Xenopus laevis* Brain Partially Rescues Developmental Defects due to PORCN Inhibition.**

A) Confocal images of stage 42 *X. laevis* brains from *X. laevis* grown in the presence of DMSO or 100μM Wnt-C59 immunostained for phospho-histone H3, a marker of actively dividing cells. Scale bar = 250μm.

B) Confocal images of stage 42 *X. laevis* brains from *X. laevis* expressing importin α modified with a c-terminal CaaX domain which forces cortical localization via farnesylation and grown in

616 the presence of 100μM Wnt-C59 immunostained for phospho-histone H3 and the modified
617 importin α-CaaX construct.
618 C) Confocal images of stage 42 *X. laevis* brains from *X. laevis* expressing an mCherry construct
619 modified with a c-terminal CaaX domain and grown in the presence of 100μM Wnt-C59
620 immunostained for phospho-histone H3 and the modified CaaX construct.
621 D) Quantification of the number of phospho-histone H3 positive cells in stage 42 *X. laevis* brains
622 of *X. laevis* grown in the presence of DMSO or 100μM Wnt-C59 and expressing importin α-
623 CaaX or mCherry-CaaX. Mean +/- SEM n>10 *=p<0.05 ****=p<0.0001. Wnt-C59 treated *X.*
624 *laevis* showed a significantly reduced number of phospho-histone H3 positive cells in the brain
625 compared to DMSO treated *X. laevis*. *X. laevis* expressing importin α-CaaX in the brain display
626 a partial rescue of the reduced phospho-histone H3 levels which was not recapitulated in *X.*
627 *laevis* expressing mCherry-CaaX.
628

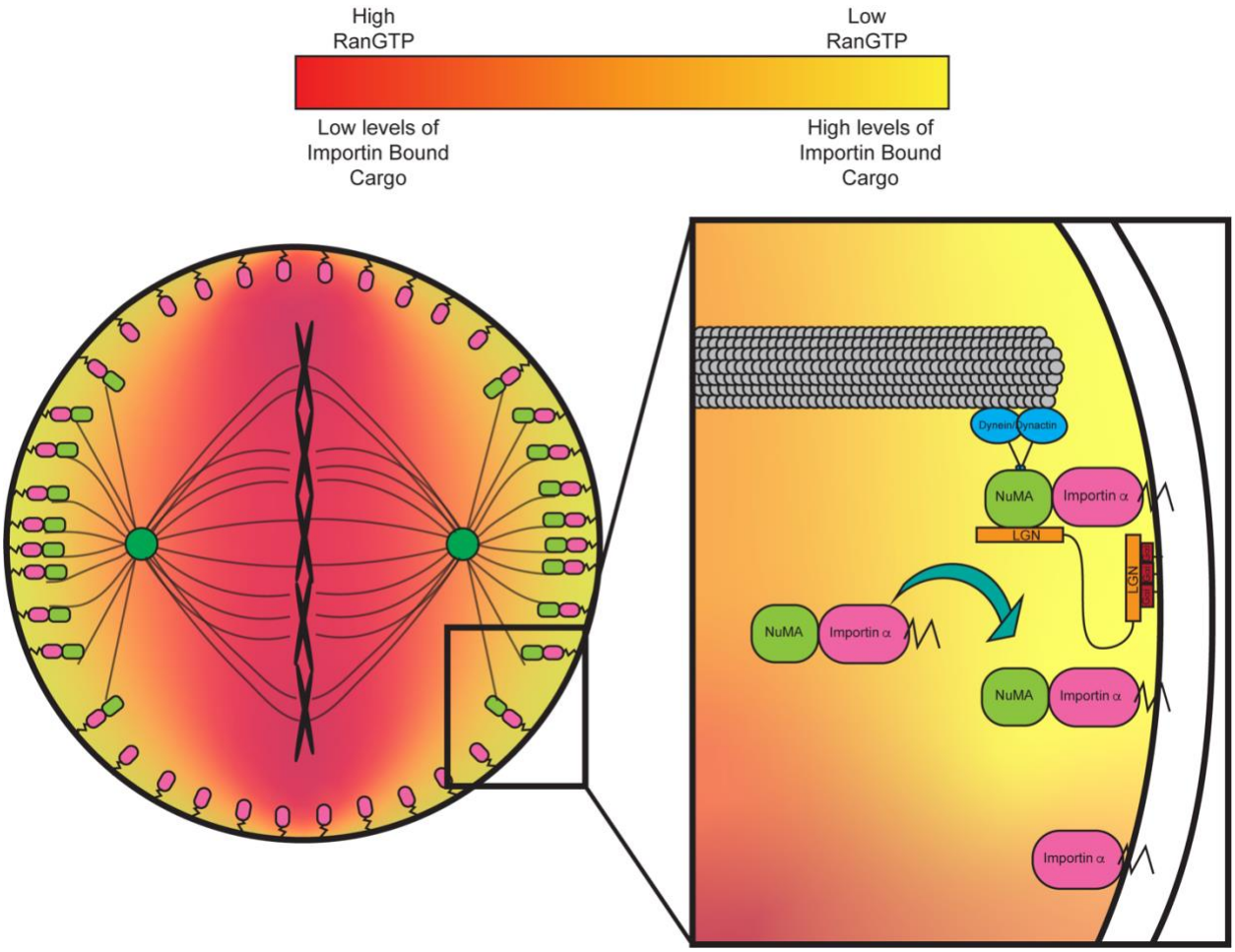


**Figure 6. Importin α regulates mitotic spindle orientation through mediating NuMA localization to the metaphase cortex and maintenance at the cell cortex through anaphase in a palmitoylation dependent manner.**

Proposed model of palmitoylated importin α's role in astral microtubule anchoring as a transporter of NuMA and a scaffold at the cell cortex for astral microtubule anchoring proteins to maintain cortical localization throughout metaphase and anaphase.

640 **RESOURCE AVAILABILITY**

641 **Lead Contact for Reagent and Resource Sharing**

642 Further information and requests for resources and reagents should be directed to and will be
643 fulfilled by the Lead Contact, Christopher W. Brownlee
644 (Christopher.Brownlee@stonybrook.edu).

645 **Materials Availability**

646 Plasmids generated in this study are being deposited to Addgene.

647 **Data and Code Availability**

648 - Microscopy data reported in this study will be shared by the lead contact upon request
649 - No original code was generated in this study
650 - Any additional information required to reanalyze the data reported in this paper is
651 available from the lead contact upon request

652

653 **EXPERIMENTAL MODEL AND SUBJECT DETAILS**

654 **Cell Culture**

655 RPE-1 and HCT116 cells were cultured as previously described (Kiyomitsu and Cheeseman,
656 2012).

657 **Animal Models**

658 All animals were maintained in accordance with standards established by the Division of
659 Laboratory Animal Resources at Stony Brook University

660

661 **METHOD DETAILS**

662 **Cell Culture and Immunostaining**

663 RPE-1 and HCT116 cells were cultured as previously described (Kiyomitsu and Cheeseman,
664 2012) in DMEM F-12 and McCoy's 5A media, respectively, supplemented with 5% FBS and
665 grown at 5% $CO_2$. Immunostaining was carried out on cells cultured onto fibronectin coated
666 coverslips, fixed with 4% PFA, permeabilized with PBS+0.2% Triton X-100 (Sigma-Aldrich
667 9036-19-5), and blocked with Bovine Serum Albumin (BSA) in PBS+0.2% Triton X-100. The
668 coverslips were than incubated with antibodies diluted in PBS+0.2% Triton X-100 as follows:
669 Rabbit polyclonal anti-NuMA 1:1000 (Novus Biologicals), monoclonal living colors antibody
670 1:1000 (Takarabio), rabbit polyclonal anti-mcherry 1:1000 (Proteintech), monoclonal anti-
671 importin α 1:1000 (Proteintech), rabbit polyclonal anti-importin α 1:1000 (ABclonal),
672 monoclonal anti-β tubulin E7 1:1000 (DSHB), monoclonal anti-SAP97 1:1000 (Enzo Life
673 Sciences), rabbit polyclonal anti-γ tubulin 1:1000 (Sigma-Aldrich), donkey anti-mouse IgG AF-
674 488 1:1000 (Southern Biotech), donkey anti-rabbit IgG AF-488 1:1000 (Southern Biotech),
675 donkey anti-mouse IgG AF-568 1:1000 (Invitrogen) and donkey anti-rabbit IgG AF-488 1:1000
676 (Invitrogen). The coverslips were then mounted onto slides with ProLong Diamond Antifade
677 Mountant (ThermoFisher P36961).

678 **Mitotic Arrest and Drug Treatment**

679 RPE-1 and HCT116 cells were arrested in metaphase through a sequential drug treatment of RO-
680 3306 and MG-132. Cells were treated with 9μM RO-3306 to arrest at the G2/M transition for 20
681 hours at 37°C. Cells were then washed with fresh media three times to remove RO-3306 and
682 treated with 20μM MG-132 within 15 minutes of RO-3306 washout to arrest cells at metaphase.
683 Cells were incubated in MG-132 for 1 hour at 37°C. In experiments with palmitoylation and
684 importin function disrupting drug treatments cells were treated with DMSO, 10μM Wnt-C59,

685 50μM palmostatin, 40μM importazole, 25μM ivermectin, or 100μM 2-bromopalmitate with the
686 MG-132 treatment and incubated for 1 hour at 37°C.

687 **Spindle Angle Measurement**

688 Mitotic spindle angles of metaphase-arrested cells were determined by measuring the vertical
689 and horizontal distances between the centrosomes at each pole of the mitotic cell and calculating
690 the arctangent of the vertical distance divided by the horizontal distance as follows:

691 $$\alpha = \arctan\left(\frac{z}{x}\right)$$

692 The vertical distance was determined through imaging the cell and measuring the length of a line
693 drawn between each centrosome. The horizontal distance was determined through using a z-stack
694 of the mitotic cell, determining at which z-slice each centrosome was in optimal focus, and
695 calculating the z distance between each slice of optimal focus. Z-stacks were taken at a step
696 distance of 0.1μm with varying numbers of steps depending on individual cell size.

697 ***X. laevis* Fertilization**

698 *Xenopus laevis* adult females were induced to lay eggs by a priming injection of 100 U of
699 pregnant mare serum gonadotropin (PMSG) at least 48 hours before use and a boosting injection
700 of 500 U of human chorionic gonadotropin (hCG) 16 hours before use. Following the hCG
701 injection, adult female *X. laevis* were placed in a 2L water bath of 1X MMR (100 mM NaCl, 2
702 mM KCl, 1 mM $MgCl_2$, 2 mM $CaCl_2$, 0.1 mM EDTA, 5 mM HEPES pH 7.8) overnight at 17°C.
703 approximately 16 hours following hCG injection, fresh eggs were collected by squeezing eggs
704 from ovulating frogs into a 10cm plastic petri dish. To fertilize eggs, a sperm solution made from
705 ¼ of a male frog testis was placed in 1mL 1X MR (100 mM NaCl, 1.8 mM KCl, 2.0 mM $CaCl_2$,
706 1.0 $MgCl_2$, 5.0 mM HEPES-NaOH, pH 7.6) and homogenized using scissors and a pestle. 1mL
707 of sperm solution was added dropwise to the freshly squeezed eggs and the dish was swirled to

708 form a monolayer of eggs and incubated for 3 mins. Dishes were flooded with milli-Q water and
709 incubated for an additional 10 mins. Eggs were dejellied with a 2% cysteine solution for 6
710 minutes with occasional swirling and washed 5 times with 1/3 MR. Fertilized eggs were
711 incubated at 23ºC until the appropriate developmental stage. In experiments where *X. laevis*
712 embryos were drug treated, the embryos were placed into a bath of 1/3 MR containing either
713 DMSO, 100µM Wnt-C59, or 1mM palmostatin 24 hours post fertilization and kept in drug bath
714 until the appropriate developmental stage for each experiment. In drug treatment conditions,
715 morphometric defects made it often difficult to determine the exact stage of Wnt-C59 and
716 palmostatin treated embryos between NF stages 40 to 43, so analysis was conducted when the
717 DMSO treated embryos were at the appropriate stage.

718 ***X. laevis* Morphometric Measurements**

719 *X. laevis* embryos were analyzed for morphometric defects at stage 42 by immobilizing embryos
720 in a bath of 140µg/mL MS-222 and imaging at 4X mounted upright. All measurements were
721 made in ImageJ. Distance between eyes was determined by measuring the straight line distance
722 from the right most portion of the left eye to the left most portion of the right eye, snout length
723 was determined by drawing a line from the front of the left eye to the right eye and then
724 measuring the straight line distance from the center of this line to the mouth, and overall head
725 area was determined by measuring the area of a circle drawn around the head such that each eye
726 is completely within the circle and the circle does not extend beyond the snout.

727 ***X. laevis* Whole Mount Immunostaining**

728 *X. laevis* embryos were fixed in 4% PFA for 24 hours at 4ºC. Following fixation, embryos were
729 immunostained by washing in PBS 3x20 min, photobleaching in a solution of 5% formamide and
730 1.2% hydrogen peroxide for 2 hours, washing in PBS + 0.1% Triton X-100 (PBST) overnight at

731 4°C, blocking with 2% BSA in PBST for 3 hours at RT, incubating with 1° antibodies diluted in
732 PBST overnight at 4°C as follows: rabbit polyclonal anti-nestin 1:1000 (Sino Biological), rabbit
733 polyclonal anti-mCherry 1:1000 (Proteintech), and monoclonal anti-phospho Histone H3 1:1000
734 (Proteintech), washing 3x1 hour in PBST, incubating with 2° antibodies diluted in PBST
735 overnight at 4°C as follows: , washing 3x1 hour in PBST and mounting onto a coverslip in
736 fluoromount G. In cases where embryos were cleared before mounting, embryos were chilled in
737 1-propanol and incubated 2x5 minutes, cleared with 5mL Murray's (2 parts Benzyl Benzoate and
738 1 part Benzyl Alcohol) and then mounted onto a coverslip with fluoromount G.

739 **Plasmid Construct Development**

740 Plasmid constructs were cloned into pCS2+ and pcDNA4TO vectors from existing plasmid
741 constructs of importin α, GFP, mCherry-CaaX, and NuMA-GFP.

742 **Embryo Microinjection**

743 Plasmid was loaded into a needle pulled from a 1mm glass capillary tube (TW100F-3, World
744 Percision Instruments) using a L/M-3P-A electrode/needle puller. Embryos were placed in a
745 mesh-bottomed plastic dish with 2.5% Ficoll in 1/3 MR and microinjected with a 2nL droplet of
746 the appropriate plasmid using a Narishige IM-400 microinjector system equipped with a MM-3
747 micromanipulator (Narishige). For stage 1 injections embryos were injected directly at the
748 animal pole, for stage 2 injections 1 blastomere was injected at the animal pole, and for stage 5
749 injections the D11 blastomere was injected at roughly the middle of the blastomere (as per
750 Moody, 1987). pCS2+ plasmids were injected at a concentration of 10ng/μL such that the final
751 concentration of plasmid delivered was 20pg. pcDNA4TO plasmids were co-injected with
752 pcDNA6TR at concentrations of 5ng/μL and 25ng/μL respectively such that the final
753 concentration of total plasmid delivered was 60pg. Following injection, embryos were placed

754 into a new dish containing 2.5% Ficoll in 1/3 MR and incubated at 23ºC for 4 hours after which
755 embryos were moved to a dish containing 1/3 MR and incubated at 23ºC until appropriate
756 developmental stage. Embryos injected with pcDNA4TO + pcDNA6TR were placed in 1/3 MR
757 containing 12.5µg/mL doxycycline to induce gene expression 4 hours post injection and
758 transferred to fresh 1/3 MR with 12.5µg/mL doxycycline 24 hours post injection.

759 ***X. laevis* Nestin Positive Cell Count**

760 Stage 46 *X. laevis* embryos were whole mount fixed and stained for DNA (Hoechst) and nestin
761 (Rb α-nestin Sino Biological 100244-T08). Embryos were imaged at 20X magnification on an
762 EVOS M7000 epifluorescent microscope to generate a z-stack image of the brain of each
763 embryo. Z-stack images were processed in Celeste Image Analysis software for 3D-
764 deconvolution to remove background signal and using a parent child analysis measured the
765 number of DNA containing cells in the brain with overlapping nestin signal in the maximum
766 projection of the processed z-stack.

767 ***X. laevis* Phospho-Histone H3 Positive Cell Count**

768 Stage 42 *X. laevis* embryos were whole mount fixed and stained for DNA (Hoechst), Phospho-
769 histone H3, and mCherry to visualize mCherry tagged proteins from microinjected constructs.
770 Whole embryos were imaged at 10X on a Zeiss LSM 980 confocal microscope by imaging a Z-
771 stack of the brain. A maximum projection image from this z-stack was then processed in Celeste
772 Image Analysis Software and a 3D count was measured in an ROI around the brain to determine
773 the number of cells positive for Phospho-histone H3 signal. Phospho-histone H3 positive cell
774 counts were determined by thresholding the minimal signal such that individual positive cells
775 could be resolved from background fluorescence.

776 **Proximity Ligation Assay**

777 Proximity ligation assay (PLA) was performed using DuoLink PLA (Millipore Sigma) following
778 the recommended protocol. PLA analysis of importin α and NuMA interaction was performed in
779 mitotically arrested HCT 116 cells using mouse anti-importin α (Proteintech) and rabbit anti-
780 NuMA (Novus Biologicals). PLA analysis of importin α and Dlg interaction was performed in
781 mitotically arrested HCT 116 cells using rabbit anti-importin α (ABclonal) and mouse anti-
782 SAP97 (Enzo Life Sciences). Cells were imaged with an EVOS M7000 epifluorescent
783 microscope at 60X magnification. Localization of PLA fluorescent signal was quantified by
784 counting the number of foci within three separate ROIs of each cell. Polar cortex ROI was
785 defined as the region from the plasma membrane at each pole to the centrosomes. Lateral cortex
786 ROI was defined as the region from the plasma membrane to the chromatin between the
787 centrosomes. Cytosol ROI was defined as the region between the centrosomes excluding the
788 plasma membrane. The number of foci in each region was calculated as a percentage of the total
789 number of foci for that cell. Cell border was determined by a brightfield image of each mitotic
790 cell quantified.

791 **Cell Lysis and Western Blot Analysis**

792 Lysates of RPE-1 and HCT 116 cells were generated from 10cm dishes seeded with $1x10^6$ cells 2
793 days prior to lysis. Cells were collected by washing with ice cold PBS and scraping off the plate
794 into solution. Cells were spun at 100xg for 5 minutes, supernatant was aspirated and cells were
795 resuspended in 150µL RIPA buffer (150 mM sodium chloride, 1.0% Triton X-100, 0.5% sodium
796 deoxycholate, 0.1% SDS, 50 mM Tris, pH 8.0) supplemented with 10µg/mL each of leupeptin,
797 pepstatin and chymostatin (LPC) protease inhibitors. Resuspended cells were rocked at $4^oC$ for 1
798 hour and spun at 12,000 rpm for 20 minutes at $4^oC$ in an Eppendorf FA-45-24-11 rotor.
799 Supernatant containing cell lysate proteins was then mixed 1:1 with 2X laemlli buffer, boiled at

100ºC for 5 minutes and stored at -20ºC until use. Western blot analysis was performed on cell lysates by running lysates through SDS-PAGE in a 7.5% or 5.0% Tris-glycine gel (dependent on size of proteins being analyzed), transferring to a nitrocellulose membrane, and blotting for target proteins. Western blot analysis for NuMA was performed with overnight transfer of SDS-PAGE gel at 20V at 4ºC while all other proteins were performed with a transfer at 150V for 90 minutes at room temperature.

**Co-Immuno Precipitation**

Co-immunoprecipitation was performed with Thermo Fisher IgG conjugated magnetic Dynabeads following recommended protocol. Cell lysates were generated for immunoprecipitation experiments with previously stated cell lysis protocol using a non-denaturing lysis buffer (20 mMTris HCl pH 8, 137 mM NaCl, 1% Triton X-100, 2 mM EDTA) in place of RIPA buffer.

**Mitotic Protein Localization Measurement**

To determine changes to KPNA2 and NuMA localization in cultured cells upon drug treatment, cells were mounted onto fibronectin coated coverslips, arrested in metaphase, drug treated, washed with cytoskeletal buffer (100mM NaCl, 300mM Sucrose, 3mM MgCl2, 10mM PIPES, pH 6.9, supplemented with 250µL 1M EGTA and 250µL Triton X-100 per 50 mL immediately before use), fixed with 4% PFA, and immunostained for DNA and KPNA2/NuMA. For KPNA2 localization cells were imaged using an EVOS M7000 at 100X with cell boundaries determined using bright-field images. For NuMA localization cells were imaged using a Leica SP5 confocal at 40X. To determine the cellular localization of target protein in each drug condition, 60 mitotic cells were imaged per drug treatment and the fluorescent intensity of KPNA2 or NuMA signal was measured in ImageJ at three cellular locations. A 10 pixel wide and 50 pixel long line was

drawn at one cortical pole, one lateral membrane, and along the midline of the cell and measured. In order to normalize variations in intensity from inconsistent immunostaining, these measurements were normalized to each other on a cell-by-cell basis by determining the ratio of polar vs lateral signal, polar vs cytosolic signal, and lateral vs cytosolic signal. In the cases where one cortical pole differed in intensity from the opposite cortical pole, the pole with the higher measure of intensity was used for data analysis (the same method was used when measuring the lateral poles).

**DNA Transfection**

HCT116 cells were seeded onto fibronectin coated coverslips. The following day media was replaced with serum free media and a mixture of 1μg plasmid in 12μL polyethylenimine (PEI) was added dropwise to cells. Cells were incubated in PEI mixture for 4 hours then media was washed out and replaced with complete media and incubated overnight before fixation and imaging.

**Subcellular Fractionation**

HCT116 cells were seeded in a 10cm dish and incubated at 37ºC. Following 2 days of incubation Cells were incubated with DMSO for 1 hour at 37ºC then lifted from dish with ice cold PBS and a cell scraper. Collected cells were then fractionated using the Minute Plasma Membrane/Protein Isolation and Cell Fractionation kit from Invent Biotechnologies following the recommended protocol.

**DNA Nucleofection**

HCT116 cells were transfected via nucleofection using LONZA SE cell line 4D-Nucleofector kit (Catalog #V4XC-1032) following recommended protocol. Following nucleofection cells were incubated for 24 hours before fixation and immunostaining for mitotic spindle angle analysis.

846 **Palmitoylation Prediction**

847 GPS-Palm (Ning et al., 2021) was employed for detection of potential palmitoylated cysteines
848 within human KPNA2. Cysteines above a threshold score of >0.6 (specificity > 85% and
849 accuracy > 82%) were considered to be likely palmitoylated.

850 **Nuclear Localization Signal, Cellular Localization, and Protein Function Prediction**

851 NucPred (Brameier et al., 2007) was used to determine which proteins in the human genome
852 contain potential NLS sequences. Any proteins above a threshold score of >0.63 (specificity >
853 71% and accuracy >53%) were considered potential NLS-sequence containing candidate
854 proteins. Proteins were then filtered to discard transmembrane proteins while retaining only
855 plasma membrane proteins, as identified by UniProt GO identifiers (Ashburner et al., 2000;
856 Aleksander et al., 2023). Proteins were then sorted by cellular localization and function using
857 GO enrichment analysis (Thomas et al., 2022).

858

859

860 **QUANTIFICATION AND STATISTICAL ANALYSIS**

861 All statistical analysis was performed in GraphPad Prism 10.0. Comparisons between datasets
862 was determined by a student's t-test unless otherwise stated. Graphs represent the mean value +/-
863 the SEM unless otherwise stated. *p<0.05 **p<0.01 ***p<0.001 ****p<0.0001 unless
864 otherwise stated.

865
866

867 **References**

868 Alam, S.M. 2018. Proximity Ligation Assay (PLA). *Curr Protoc Immunol*. 123.
869 doi:10.1002/cpim.58.Proximity.

870 Aleksander, S.A., J. Balhoff, S. Carbon, J.M. Cherry, H.J. Drabkin, D. Ebert, M. Feuermann, P.
871 Gaudet, N.L. Harris, D.P. Hill, R. Lee, H. Mi, S. Moxon, C.J. Mungall, A. Muruganugan, T.
872 Mushayahama, P.W. Sternberg, P.D. Thomas, K. Van Auken, J. Ramsey, D.A. Siegele,
873 R.L. Chisholm, P. Fey, M.C. Aspromonte, M.V. Nugnes, F. Quaglia, S. Tosatto, M. Giglio,
874 S. Nadendla, G. Antonazzo, H. Attrill, G. Dos Santos, S. Marygold, V. Strelets, C.J.
875 Tabone, J. Thurmond, P. Zhou, S.H. Ahmed, P. Asanitthong, D. Luna Buitrago, M.N.
876 Erdol, M.C. Gage, M. Ali Kadhum, K.Y.C. Li, M. Long, A. Michalak, A. Pesala, A.
877 Pritazahra, S.C.C. Saverimuttu, R. Su, K.E. Thurlow, R.C. Lovering, C. Logie, S.
878 Oliferenko, J. Blake, K. Christie, L. Corbani, M.E. Dolan, L. Ni, D. Sitnikov, C. Smith, A.
879 Cuzick, J. Seager, L. Cooper, J. Elser, P. Jaiswal, P. Gupta, S. Naithani, M. Lera-Ramirez,
880 K. Rutherford, V. Wood, J.L. De Pons, M.R. Dwinell, G.T. Hayman, M.L. Kaldunski, A.E.
881 Kwitek, S.J.F. Laulederkind, M.A. Tutaj, M. Vedi, S.J. Wang, P. D'Eustachio, L. Aimo, K.
882 Axelsen, A. Bridge, N. Hyka-Nouspikel, A. Morgat, S.R. Engel, K. Karra, S.R. Miyasato,
883 R.S. Nash, M.S. Skrzypek, S. Weng, E.D. Wong, E. Bakker, T.Z. Berardini, L. Reiser, A.
884 Auchincloss, G. Argoud-Puy, et al. 2023. The Gene Ontology knowledgebase in 2023.
885 *Genetics*. 224:1–14. doi:10.1093/genetics/iyad031.
886 Ashburner, M., C.A. Ball, J.A. Blake, D. Botstein, H. Butler, J.M. Cherry, A.P. Davis, K.
887 Dolinski, S.S. Dwight, J.T. Eppig, M.A. Harris, D.P. Hill, L.I.-T.A. Kasarskis, S. Lewis,
888 J.C. Matese, J.E. Richardson, M. Ringwald, G.M. Rubin, and G. Sherlock. 2000. Gene
889 Ontology: tool for the unification of biology. *Nat. Genet.* 25:25–29.
890 doi:10.2174/1381612824666180522105202.
891 Bergstralh, D.T., N.S. Dawney, and D. St Johnston. 2017. Spindle orientation: A question of
892 complex positioning. *Dev.* 144:1137–1145. doi:10.1242/dev.140764.

893 Bergstralh, D.T., H.E. Lovegrove, I. Kujawiak, N.S. Dawney, J. Zhu, S. Cooper, R. Zhang, and
894 D.S. Johnston. 2016. Pins is not required for spindle orientation in the drosophila wing disc.
895 *Dev.* 143:2573–2581. doi:10.1242/dev.135475.
896 Bergstralh, D.T., and D. St Johnston. 2014. Spindle orientation: What if it goes wrong? *Semin.*
897 *Cell Dev. Biol.* 34:140–145. doi:10.1016/j.semcdb.2014.06.014.
898 Bowman, S.K., R.A. Neumüller, M. Novatchkova, Q. Du, and J.A. Knoblich. 2006. The
899 Drosophila NuMA Homolog Mud Regulates Spindle Orientation in Asymmetric Cell
900 Division. *Dev. Cell*. 10:731–742. doi:10.1016/j.devcel.2006.05.005.
901 Brameier, M., A. Krings, and R.M. MacCallum. 2007. NucPred - Predicting nuclear localization
902 of proteins. *Bioinformatics*. 23:1159–1160. doi:10.1093/bioinformatics/btm066.
903 Brownlee, C., and R. Heald. 2019. Importin α Partitioning to the Plasma Membrane Regulates
904 Intracellular Scaling. *Cell*. 176:805-815.e8. doi:10.1016/j.cell.2018.12.001.
905 Camuglia, J., S. Chanet, and A.C. Martin. 2022. Morphogenetic forces planar polarize LGN/Pins
906 in the embryonic head during Drosophila gastrulation. *bioRxiv*. 2022.01.07.475359.
907 Carvalho, C.A., S. Moreira, G. Ventura, C.E. Sunkel, and E. Morais-De-Sá. 2015. Aurora a
908 triggers Lgl cortical release during symmetric division to control planar spindle orientation.
909 *Curr. Biol.* 25:53–60. doi:10.1016/j.cub.2014.10.053.
910 Chang, C.C., T.L. Huang, Y. Shimamoto, S.Y. Tsai, and K.C. Hsia. 2017. Regulation of mitotic
911 spindle assembly factor NuMA by Importin-β. *J. Cell Biol.* 216:3453–3462.
912 doi:10.1083/jcb.201705168.
913 Charnley, M., F. Anderegg, R. Holtackers, M. Textor, and P. Meraldi. 2013. Effect of Cell Shape
914 and Dimensionality on Spindle Orientation and Mitotic Timing. *PLoS One*. 8.
915 doi:10.1371/journal.pone.0066918.

916 Chhabra, S.N., and B.W. Booth. 2021. Asymmetric cell division of mammary stem cells. *Cell*
917 *Div.* 16:1–15. doi:10.1186/s13008-021-00073-w.
918 Dekker, F.J., O. Rocks, N. Vartak, S. Menninger, C. Hedberg, R. Balamurugan, S. Wetzel, S.
919 Renner, M. Gerauer, B. Schölermann, M. Rusch, J.W. Kramer, D. Rauh, G.W. Coates, L.
920 Brunsveld, P.I.H. Bastiaens, and H. Waldmann. 2010. Small-molecule inhibition of APT1
921 affects Ras localization and signaling. *Nat. Chem. Biol.* 6:449–456.
922 doi:10.1038/nchembio.362.
923 Du, Q., and I.G. Macara. 2004. Mammalian Pins is a conformational switch that links NuMA to
924 heterotrimeric G proteins. *Cell*. 119:503–516. doi:10.1016/j.cell.2004.10.028.
925 Elmaci, I., M.A. Altinoz, R. Sari, and F.H. Bolukbasi. 2018. Phosphorylated Histone H3 (PHH3)
926 as a Novel Cell Proliferation Marker and Prognosticator for Meningeal Tumors: A Short
927 Review. *Appl. Immunohistochem. Mol. Morphol.* 26:627–631.
928 doi:10.1097/PAI.0000000000000499.
929 Ems-McClung, S.C., M. Emch, S. Zhang, S. Mahnoor, L.N. Weaver, and C.E. Walczak. 2020.
930 RanGTP induces an effector gradient of XCTK2 and importin α/β for spindle microtubule
931 cross-linking. *J. Cell Biol.* 219:1–15. doi:10.1083/jcb.201906045.
932 Exner, C.R.T., and H.R. Willsey. 2021. Xenopus leads the way: Frogs as a pioneering model to
933 understand the human brain. *Genesis*. 59. doi:10.1002/dvg.23405.
934 Fankhaenel, M., F. Sadat Golestan Hashemi, M. Mosa Hosawi, L. Mourao, P. Skipp, X. Morin,
935 C. LGJ Scheele, and S. Elias. 2023. Annexin A1 is a polarity cue that directs planar mitotic
936 spindle orientation during mammalian epithelial morphogenesis. *bioRxiv*. 454117.
937 doi:10.1038/s41467-023-35881-x.
938 Finegan, T.M., and D.T. Bergstralh. 2019. Division orientation: disentangling shape and

939 mechanical forces. *Cell Cycle*. 18:1187–1198. doi:10.1080/15384101.2019.1617006.
940 Gallini, S., M. Carminati, F. De Mattia, I.A. Asteriti, and G. Guarguaglini. 2016. NuMA
941 Phosphorylation by Aurora-A Orchestrates Spindle Orientation. *Curr. Biol.* 26:458–469.
942 doi:10.1016/j.cub.2015.12.051.
943 Goldfarb, D.S., A.H. Corbett, D.A. Mason, M.T. Harreman, and S.A. Adam. 2004. Importin α: A
944 multipurpose nuclear-transport receptor. *Trends Cell Biol.* 14:505–514.
945 doi:10.1016/j.tcb.2004.07.016.
946 Guan, X., and C.A. Fierke. 2011. Understanding protein palmitoylation: Biological significance
947 and enzymology. *Sci. China Chem.* 54:1888–1897. doi:10.1007/s11426-011-4428-2.
948 He, S., J.P. Gillies, J.L. Zang, C.M. Córdoba-Beldad, I. Yamamoto, Y. Fujiwara, J. Grantham,
949 M.E. DeSantis, and H. Shibuya. 2023. Distinct dynein complexes defined by DYNLRB1
950 and DYNLRB2 regulate mitotic and male meiotic spindle bipolarity. *Nat. Commun.* 14:1–
951 15. doi:10.1038/s41467-023-37370-7.
952 Higgins, C.D., and B. Goldstein. 2010. Asymmetric cell division: A new way to divide
953 unequally. *Curr. Biol.* 23:R1029–R1031. doi:10.1016/j.earlhumdev.2006.05.022.
954 Kalab, P., and R. Heald. 2008. The RanGTP gradient - A GPS for the mitotic spindle. *J. Cell Sci.*
955 121:1577–1586. doi:10.1242/jcs.005959.
956 Kaláb, P., A. Pralle, E.Y. Isacoff, R. Heald, and K. Weis. 2006. Analysis of a RanGTP-regulated
957 gradient in mitotic somatic cells. *Nature*. 440:697–701. doi:10.1038/nature04589.
958 Kennedy, A.E., and A.J. Dickinson. 2014. Quantification of orofacial phenotypes in xenopus. *J.*
959 *Vis. Exp.* 1–14. doi:10.3791/52062.
960 Kiyomitsu, T., and S. Boerner. 2021. The Nuclear Mitotic Apparatus (NuMA) Protein: A Key
961 Player for Nuclear Formation, Spindle Assembly, and Spindle Positioning. *Front. Cell Dev.*

962 *Biol.* 9:1–12. doi:10.3389/fcell.2021.653801.

963 Kiyomitsu, T., and I.M. Cheeseman. 2012. Chromosome-and spindle-pole-derived signals
964 generate an intrinsic code for spindle position and orientation. *Nat. Cell Biol.* 14:311–317.
965 doi:10.1038/ncb2440.

966 Kiyomitsu, T., and I.M. Cheeseman. 2013. XCortical dynein and asymmetric membrane
967 elongation coordinately position the spindle in anaphase. *Cell*. 154:391.
968 doi:10.1016/j.cell.2013.06.010.

969 Konno, D., G. Shioi, A. Shitamukai, A. Mori, H. Kiyonari, T. Miyata, and F. Matsuzaki. 2008.
970 Neuroepithelial progenitors undergo LGN-dependent planar divisions to maintain self-
971 renewability during mammalian neurogenesis. *Nat. Cell Biol.* 10:93–101.
972 doi:10.1038/ncb1673.

973 Kotak, S., and P. Gönczy. 2013. Mechanisms of spindle positioning: Cortical force generators in
974 the limelight. *Curr. Opin. Cell Biol.* 25:741–748. doi:10.1016/j.ceb.2013.07.008.

975 Lasser, M., B. Pratt, C. Monahan, S.W. Kim, and L.A. Lowery. 2019. The many faces of
976 Xenopus: Xenopus laevisas a model system to study Wolf-Hirschhorn syndrome. *Front.*
977 *Physiol.* 10:1–12. doi:10.3389/fphys.2019.00817.

978 Lin, D.T.S., and E. Conibear. 2015. ABHD17 proteins are novel protein depalmitoylases that
979 regulate N-Ras palmitate turnover and subcellular localization. *Elife*. 4:1–14.
980 doi:10.7554/eLife.11306.

981 Mariscal, J., T. Vagner, M. Kim, B. Zhou, A. Chin, M. Zandian, M.R. Freeman, S. You, A.
982 Zijlstra, W. Yang, and D. Di Vizio. 2020. Comprehensive palmitoyl-proteomic analysis
983 identifies distinct protein signatures for large and small cancer-derived extracellular
984 vesicles. *J. Extracell. Vesicles*. 9. doi:10.1080/20013078.2020.1764192.

985 Moody, S.A. 1987a. Fates of the blastomeres of the 16-cell stage Xenopus embryo. *Dev. Biol.*
986 119:560–578. doi:10.1016/0012-1606(87)90059-5.
987 Moody, S.A. 1987b. Fates of the blastomeres of the 32-cell-stage Xenopus embryo. *Dev. Biol.*
988 122:300–319. doi:10.1016/0012-1606(87)90296-X.
989 Neville, K.E., T.M. Finegan, N. Lowe, P.M. Bellomio, D. Na, and D.T. Bergstralh. 2022. The
990 Drosophila mitotic spindle orientation machinery requires activation, not just localization.
991 *bioRxiv*.
992 Ning, W., P. Jiang, Y. Guo, C. Wang, X. Tan, W. Zhang, D. Peng, and Y. Xue. 2021. GPS-Palm:
993 A deep learning-based graphic presentation system for the prediction of S-palmitoylation
994 sites in proteins. *Brief. Bioinform.* 22:1836–1847. doi:10.1093/bib/bbaa038.
995 Oka, M., and Y. Yoneda. 2018. Importin α: Functions as a nuclear transport factor and beyond.
996 *Proc. Japan Acad. Ser. B Phys. Biol. Sci.* 94:259–274. doi:10.2183/pjab.94.018.
997 Okumura, M., T. Natsume, M.T. Kanemaki, and T. Kiyomitsu. 2018. Dynein–dynactin–NuMA
998 clusters generate cortical spindle-pulling forces as a multiarm ensemble. *Elife*. 7:1–24.
999 doi:10.7554/eLife.36559.
1000 Ozugergin, I., and A. Piekny. 2021. Complementary functions for the Ran gradient during
1001 division. *Small GTPases*. 12:177–187. doi:10.1080/21541248.2020.1725371.
1002 Pietro, F., A. Echard, and X. Morin. 2016. Regulation of mitotic spindle orientation: an
1003 integrated view. *EMBO Rep.* 17:1106–1130. doi:10.15252/embr.201642292.
1004 Pirovano, L., S. Culurgioni, M. Carminati, A. Alfieri, S. Monzani, V. Cecatiello, C. Gaddoni, F.
1005 Rizzelli, J. Foadi, S. Pasqualato, and M. Mapelli. 2019. Hexameric NuMA:LGN structures
1006 promote multivalent interactions required for planar epithelial divisions. *Nat. Commun.* 10.
1007 doi:10.1038/s41467-019-09999-w.

1008 Proffitt, K.D., B. Madan, Z. Ke, V. Pendharkar, L. Ding, M.A. Lee, R.N. Hannoush, and D.M.
1009 Virshup. 2013. Pharmacological inhibition of the Wnt acyltransferase PORCN prevents
1010 growth of WNT-driven mammary cancer. *Cancer Res.* 73:502–507. doi:10.1158/0008-
1011 5472.CAN-12-2258.
1012 Razuvaeva, A. V., L. Graziadio, V. Palumbo, G.A. Pavlova, J. V. Popova, A. V. Pindyurin, S.
1013 Bonaccorsi, M.P. Somma, and M. Gatti. 2023. The Multiple Mitotic Roles of the ASPM
1014 Orthologous Proteins: Insight into the Etiology of ASPM-Dependent Microcephaly. *Cells*.
1015 12:922. doi:10.3390/cells12060922.
1016 Saadaoui, M., M. Machicoane, F. di Pietro, F. Etoc, A. Echard, and X. Morin. 2014. Dlg1
1017 controls planar spindle orientation in the neuroepithelium through direct interaction with
1018 LGN. *J. Cell Biol.* 206:707–717. doi:10.1083/jcb.201405060.
1019 Schelar, E. and, and J. Liu. 2008. 基因的改变NIH Public Access. *Bone*. 23:1–7.
1020 doi:10.1038/nmeth.1293.Large-Scale.
1021 Schiller, E.A., and D.T. Bergstralh. 2021. Interaction between Discs large and
1022 Pins/LGN/GPSM2: a comparison across species. *Biol. Open*. 10:1–10.
1023 doi:10.1242/bio.058982.
1024 Serwa, R.A., F. Abaitua, E. Krause, E.W. Tate, and P. O'Hare. 2015. Systems Analysis of
1025 Protein Fatty Acylation in Herpes Simplex Virus-Infected Cells Using Chemical
1026 Proteomics. *Chem. Biol.* 22:1008–1017. doi:10.1016/j.chembiol.2015.06.024.
1027 Shantanam, S., and MUELLER. 2018. Modeling human craniofacial disorders in Xenopus.
1028 *Physiol. Behav.* 176:139–148. doi:10.1007/s40139-017-0128-8.Modeling.
1029 Singh, D., N. Schmidt, F. Müller, T. Bange, and A.W. Bird. 2021. Destabilization of Long Astral
1030 Microtubules via Cdk1-Dependent Removal of GTSE1 from Their Plus Ends Facilitates

1031 Prometaphase Spindle Orientation. *Curr. Biol.* 31:766-781.e8.
1032 doi:10.1016/j.cub.2020.11.040.
1033 Sobocinska, J., P. Roszczenko-Jasinska, M. Zareba-Kozio, A. Hromada-Judycka, O. V.
1034 Matveichuk, G. Traczyk, K. Ukasiuk, and K. Kwiatkowska. 2018. Lipopolysaccharide
1035 Upregulates Palmitoylated Enzymes of the Phosphatidylinositol Cycle: An Insight from
1036 Proteomic Studies. *Mol. Cell. Proteomics*. 17:233–254. doi:10.1074/mcp.RA117.000050.
1037 Soderholm, J.F., S.L. Bird, P. Kalab, Y. Sampathkumar, K. Hasegawa, M. Uehara-Bingen, K.
1038 Weis, and R. Heald. 2011. Importazole, a small molecule inhibitor of the transport receptor
1039 importin-β. *ACS Chem Biol*. 6:700–708. doi:10.1016/j.earlhumdev.2006.05.022.
1040 Suzuki, S., J. Namiki, S. Shibata, Y. Mastuzaki, and H. Okano. 2010. The neural stem/progenitor
1041 cell marker nestin is expressed in proliferative endothelial cells, but not in mature
1042 vasculature. *J. Histochem. Cytochem.* 58:721–730. doi:10.1369/jhc.2010.955609.
1043 Takeda, E., T. Murakami, G. Matsuda, H. Murakami, T. Zako, M. Maeda, and Y. Aida. 2011.
1044 Nuclear exportin receptor cas regulates the NPI-1-mediated nuclear import of HIV-1 vpr.
1045 *PLoS One*. 6. doi:10.1371/journal.pone.0027815.
1046 Tamanoi, F., C.L. Gau, C. Jiang, H. Edamatsu, and J. Kato-Stankiewicz. 2001. Protein
1047 farnesylation in mammalian cells: Effects of farnesyltransferase inhibitors on cancer cells.
1048 *Cell. Mol. Life Sci.* 58:1636–1649. doi:10.1007/PL00000802.
1049 Tang, X., J.J. Punch, and W.L. Lee. 2009. A CAAX motif can compensate for the PH domain of
1050 Num1 for cortical dynein attachment. *Cell Cycle*. 8:3182–3190. doi:10.4161/cc.8.19.9731.
1051 Taverna, E., M. Götz, and W.B. Huttner. 2014. The cell biology of neurogenesis: toward an
1052 understanding of the development and evolution of the neocortex. 30. 465–502 pp.
1053 Thinon, E., J.P. Fernandez, H. Molina, and H.C. Hang. 2018. Selective Enrichment and Direct

1054 Analysis of Protein S-Palmitoylation Sites. *J. Proteome Res.* 17:1907–1922.
1055 doi:10.1021/acs.jproteome.8b00002.
1056 Thomas, P.D., D. Ebert, A. Muruganujan, T. Mushayahama, L.P. Albou, and H. Mi. 2022.
1057 PANTHER: Making genome-scale phylogenetics accessible to all. *Protein Sci.* 31:8–22.
1058 doi:10.1002/pro.4218.
1059 Toyoshima, F., and E. Nishida. 2007. Integrin-mediated adhesion orients the spindle parallel to
1060 the substratum in an EB1- and myosin X-dependent manner. *EMBO J.* 26:1487–1498.
1061 doi:10.1038/sj.emboj.7601599.
1062 Tsuchiya, K., H. Hayashi, M. Nishina, M. Okumura, Y. Sato, M.T. Kanemaki, G. Goshima, and
1063 T. Kiyomitsu. 2021. Ran-GTP Is Non-essential to Activate NuMA for Mitotic Spindle-Pole
1064 Focusing but Dynamically Polarizes HURP Near Chromosomes. *Curr. Biol.* 31:115-127.e3.
1065 doi:10.1016/j.cub.2020.09.091.
1066 Wagstaff, K.M., H. Sivakumaran, S.M. Heaton, D. Harrich, and D.A. Jans. 2012. Ivermectin is a
1067 specific inhibitor of importin α/β-mediated nuclear import able to inhibit replication of
1068 HIV-1 and dengue virus. *Biochem. J.* 443:851–856. doi:10.1042/BJ20120150.
1069 Weaver, L.N., and C.E. Walczak. 2015. Spatial gradients controlling spindle assembly. *Biochem.*
1070 *Soc. Trans.* 43:7–12. doi:10.1042/BST20140243.
1071 Won, S.J., and B.R. Martin. 2018. Temporal Profiling Establishes a Dynamic S-Palmitoylation
1072 Cycle. *ACS Chem. Biol.* 13:1560–1568. doi:10.1021/acschembio.8b00157.
1073 Yang, Y., M. Liu, D. Li, J. Ran, J. Gao, S. Suo, S. Sun-Cong, and J. Zhou. 2014. CYLD
1074 regulates spindle orientation by stabilizing astral microtubules and promoting dishevelled-
1075 NuMA-dynein/ dynactin complex formation. *Proc. Natl. Acad. Sci. U. S. A.* 111:2158–
1076 2163. doi:10.1073/pnas.1319341111.

1077 Yu, F., X. Morin, Y. Cai, X. Yang, and W. Chia. 2000. Analysis of partner of inscuteable, a
1078 novel player of Drosophila asymmetric divisions, reveals two distinct steps in inscuteable
1079 apical localization. *Cell*. 100:399–409. doi:10.1016/S0092-8674(00)80676-5.
1080 Yu, M., K. Qin, J. Fan, G. Zhao, P. Zhao, W. Zeng, C. Chen, A. Wang, Y. Wang, J. Zhong, Y.
1081 Zhu, W. Wagstaff, R.C. Haydon, H.H. Luu, S. Ho, M.J. Lee, J. Strelzow, R.R. Reid, and
1082 T.C. He. 2024. The evolving roles of Wnt signaling in stem cell proliferation and
1083 differentiation, the development of human diseases, and therapeutic opportunities. *Genes*
1084 *Dis.* 11:101026. doi:10.1016/j.gendis.2023.04.042.
1085 Zheng, Z., Q. Wan, J. Liu, H. Zhu, X. Chu, and Q. Du. 2013. Evidence for dynein and astral
1086 microtubule-mediated cortical release and transport of Gαi/LGN/NuMA complex in mitotic
1087 cells. *Mol. Biol. Cell*. 24:901–913. doi:10.1091/mbc.E12-06-0458.
1088 Zhong, T., X. Gongye, M. Wang, and J. Yu. 2022. Understanding the underlying mechanisms
1089 governing spindle orientation : How far are we from there ? 1–7. doi:10.1111/jcmm.17526.
1090 Zhou, B., Y. Wang, Y. Yan, J. Mariscal, D. Di Vizio, M.R. Freeman, and W. Yang. 2019. Low-
1091 background acyl-biotinyl exchange largely eliminates the coisolation of non- s-acylated
1092 proteins and enables deep s-acylproteomic analysis. *Anal. Chem.* 91:9858–9866.
1093 doi:10.1021/acs.analchem.9b01520.
1094